Quaternary Science Advances 13 (2024) 100124

Contents lists available at ScienceDirect

Quaternary Science Advances

journal homepage: www.sciencedirect.com/journal/quaternary-science-advances

A regional assessment of the deglaciation history of the Swiss Plateau based on newly obtained and re-evaluated Be-10 cosmic-ray exposure ages

Felix Martin Hofmann [a,*], Alexander R. Groos [b,c], Ezequiel Garcia Morabito [b,d], Julian Struck [b,d,e], Christian Gnägi [f], Andreas Scharf [g], Georg Rugel [g], Silke Merchel [g,h], Roland Zech [b,d,e]

[a] Institute of Earth and Environmental Sciences, Albert-Ludwigs-Universität Freiburg, Albertstraße 23b, 79104, Freiburg im Breisgau, Germany
[b] Institute of Geography, Universität Bern, Hallerstrasse 12, 3012, Bern, Switzerland
[c] Institute of Geography, Friedrich-Alexander-Universität Erlangen-Nürnberg, Wetterkreuz 15, 91058, Erlangen, Germany
[d] Oeschger Center for Climate Change Research, Universität Bern, Hochschulstrasse 4, 3012, Bern, Switzerland
[e] Institute of Geography, Friedrich-Schiller-Universität Jena, Löbdergraben 32, 07743, Jena, Germany
[f] weg>punkt, Länggasse 7, 3360, Herzogenbuchsee, Switzerland
[g] Helmholtz-Zentrum Dresden – Rossendorf, Bautzner Landstraße 400, 01328, Dresden, Germany
[h] University of Vienna, Faculty of Physics, Isotope Physics, Währinger Straße 17, 1090, Vienna, Austria

ARTICLE INFO

Keywords:
Terrestrial in situ cosmogenic nuclides
Exposure dating
Moraine
Erratic boulder
Swiss Plateau
Deglaciation
Glacier fluctuations

ABSTRACT

During marine oxygen isotope stage (MIS) 2, the Swiss Plateau temporarily hosted large piedmont lobe glaciers that retreated after their maximum advance back to the fringe of the Alps. The presence of moraines in this region indicates that overall glacier recession was punctuated by repeated phases of ice-marginal stability and re-advances. The timing of these events in the region formerly covered by the eastern lobe of the Rhône (or Valais) glacier has been controversial and remains poorly constrained due to the lack of chronological data. To fill this gap, ^{10}Be cosmic-ray exposure (CRE) dating was applied to erratic boulders inside the assumed MIS 2 maximum extent of this piedmont lobe. An erratic boulder at an ice-marginal position upstream from the suspected MIS 2 maximum extent gave an age of about 19 ka. Erratic boulders at a presumably younger ice-marginal position (Brästenberg position) yielded an average age of ca. 20 ka. However, several erratic boulders beyond the Brästenberg position gave internally consistent, but stratigraphically too young ages of ca. 17 ka. We cannot rule out that glacier recession from the Brästenberg position began no later than 17 ka. CRE dating of a moraine of a presumably younger ice-marginal position (Solothurn position) gave unrealistically old ages and an incredibly young age (86 ka, 40 ka, and 4 ka). Carbon-14 CRE dating should be applied to provide additional information on the last deglaciation of the Swiss Plateau. Nevertheless, despite outlying ages, the presented chronological data contribute to an overall consistent and increasingly refined chronology of the last deglaciation of the Swiss Plateau when compared with 59 previously published CRE ages.

1. Introduction

The western Swiss Plateau is one of the birthplaces of the theory of glaciations during the 19th century. Studer (1825) first described the conspicuous, up to 1200 m^3-large boulders (Ivy-Ochs et al., 2021) around the hamlet of Steinhof on the western Swiss Plateau. He inferred from the lithology of the boulders (green hornblende granitic gneisses; Zimmermann, 1963) that the boulders originate from the Valais and concluded that massive floods must have transported the boulders to the Swiss Plateau. Based on discussions with Jean-Pierre Perraudin and Ignaz Vernetz, de Charpentier (1841) came up with a different theory and proposed that glaciers transported the boulders from the Valais. The glaciation hypothesis was particularly promoted by Louis Agassiz and eventually became a widely accepted paradigm (Krüger, 2008).

Since the first studies on glaciations of the western part of the Swiss Plateau, multiple studies have focused on determining the extent and

* Corresponding author.
E-mail addresses: felix.martin.hofmann@geologie.uni-freiburg.de (F.M. Hofmann), alexander.groos@fau.de (A.R. Groos), ezequiel.morabito@gmx.ch (E. Garcia Morabito), julian.struck@uni-jena.de (J. Struck), christian.gnaegi@weg-punkt.ch (C. Gnägi), g.rugel@hzdr.de (G. Rugel), silke.merchel@univie.ac.at (S. Merchel), roland.zech@uni-jena.de (R. Zech).

https://doi.org/10.1016/j.qsa.2023.100124
Received 28 June 2023; Received in revised form 18 September 2023; Accepted 19 September 2023
Available online 28 September 2023

timing of glaciations in this region. Starting with pioneering studies in the 1990s, cosmic-ray exposure (CRE) and luminescence dating particularly increased the understanding of glacier variations in this region (e.g., Ivy-Ochs, 1996; Preusser, 1999) and resulted in a large body of chronological datasets (see Ivy-Ochs et al., 2008, Preusser et al., 2011, Heiri et al., 2014; Ivy-Ochs, 2015 for detailed syntheses of previous work). Radiocarbon and luminescence ages indicate that the last maximum advance of several glaciers from the Alps to the Swiss Plateau culminated at ca. 25 ka (Keller and Krayss, 2005; Preusser et al., 2007, 2011; Gaar et al., 2019; Kamleitner et al., 2023), i.e., during marine oxygen isotope stage (MIS) 2 (29-14 ka; Lisiecki and Raymo, 2005). During this glacial phase, the Swiss Plateau hosted large piedmont lobe glaciers. These were, from the west to the east, the Rhône glacier *sensu* Kelly et al. (2004), also referred to as Valais glacier (e.g., Ivy-Ochs et al., 2021), as well as the Aare, Reuss, Linth, and Rhine glaciers (Fig. 1; see also Bini et al., 2009). The western lobe of the Rhône valley glacier flowed in a westward direction towards the city of Lyon (Fig. 1; Coutterand et al., 2009; Jouvet et al., 2017), whereas the eastern lobe extended in a north-easterly direction towards the area around the town of Wangen and merged with the Aare glacier (Ivy-Ochs et al., 2021). As emphasised by Schwenk et al. (2022), the eastern lobe of the Rhône glacier was mainly fed by ice from the accumulation area of the Rhône glacier (situated south of the ice divide in the Alps; Florineth and Schlüchter, 2000; Kelly et al., 2004) and only a small part of the ice originated from the north-western Bernese Alps, the accumulation area of the Aare glacier.

Piedmont lobe glaciers on the Swiss Plateau withdrew stepwise from their MIS 2 maximum positions (e.g., Ivy-Ochs et al., 2008; Reber et al., 2014; Kamleitner et al., 2023). Ice surface lowering in the interior of the Alps began at around 18.5 ka (Wirsig et al., 2016a). Overall glacier recession during the last glacial termination, informally defined as the period between the Last Glacial Maximum (LGM; at 27.5—23.3 ka based on the terrestrial stratigraphic record; Hughes and Gibbard, 2015) and the onset of the Holocene (11.7 ka; Cohen and Gibbard, 2019), was punctuated by glacier re-advances, oscillations, and standstills. Glacier re-advances occurred during the Gschnitz and the Egesen stadials. Moraines that formed during these periods of glacier expansion have been dated to ca. 18 ka and 13—11 ka, respectively, at multiple sites across the Alps (e.g., Ivy-Ochs et al., 2006a, b; Boxleitner et al., 2019; Hofmann et al., 2019).

Apart from these well-known periods of glacier expansion, phases of ice-marginal stability occurred during the early phase of deglaciation, testified by widespread moraines on the Swiss Plateau (Institut für Geologie, Universität Bern, Bundesamt für Wasser und Geologie, 2005). The age of some of these landforms has already been determined with CRE dating (Akçar et al., 2011; Reber et al., 2014; Wüthrich et al., 2018; Kamleitner et al., 2023). Despite its great success, CRE dating of erratic boulders on the Swiss Plateau has proven to be problematic, as many erratic boulders in this region have been destroyed and removed from fields for agricultural purposes (cf., Akçar et al., 2011; Ivy-Ochs et al., 2021). Although erratic boulders have been protected by law as early as in 1868 CE, their distribution is nowadays mainly restricted to forest areas (Maurer, 2005).

As shown in Fig. 2, multiple ice-marginal positions of the eastern lobe of the Rhône glacier have been described in the literature. The outermost ice-marginal positions are the Langenthal and Niederbipp

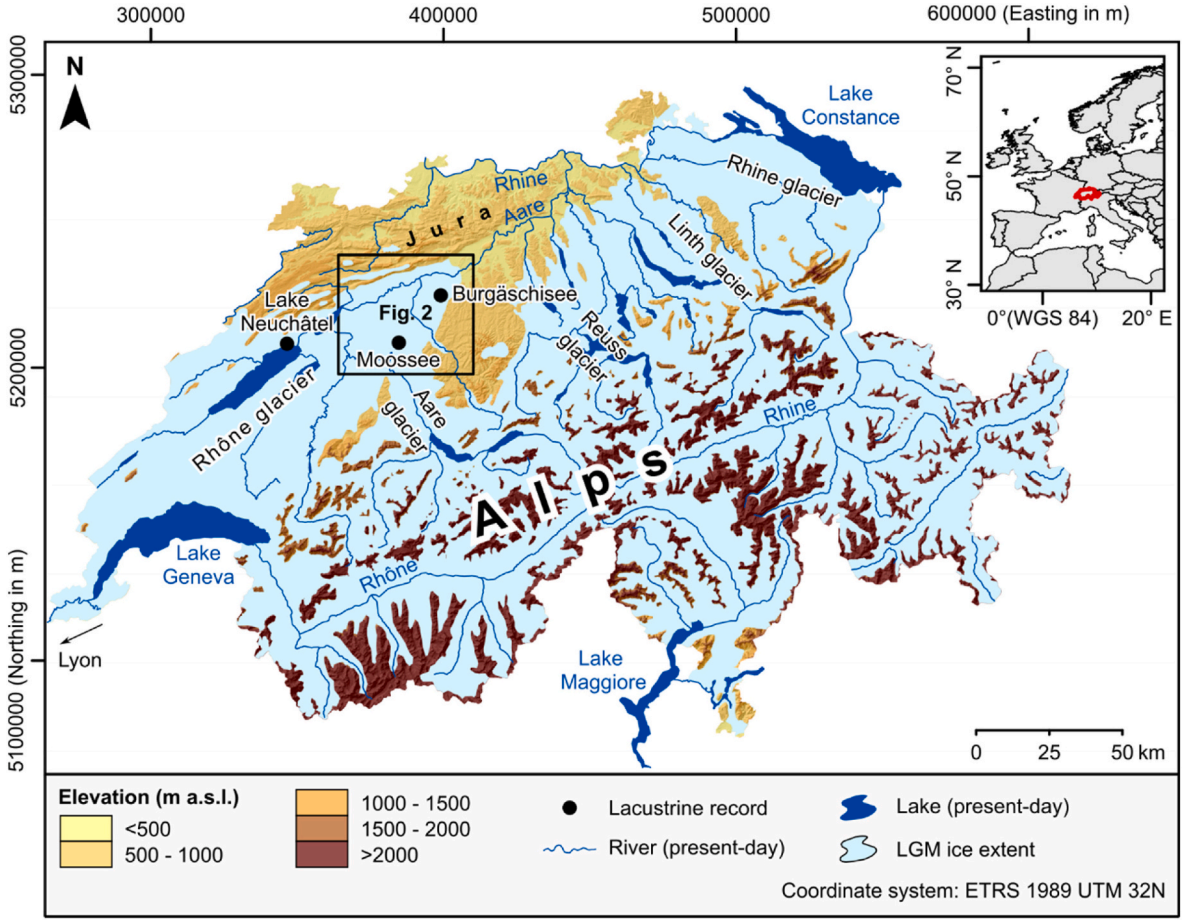

Fig. 1. Location of the study area and ice extent in Switzerland during the last glacial maximum *sensu* Ehlers et al. (2011). The ice extent was superimposed on a digital elevation model derived from data of the shuttle radar topography mission (NASA Jet Propulsion Laboratory, 2013). © BFS, ThemaKart 2022 for rivers and lakes.

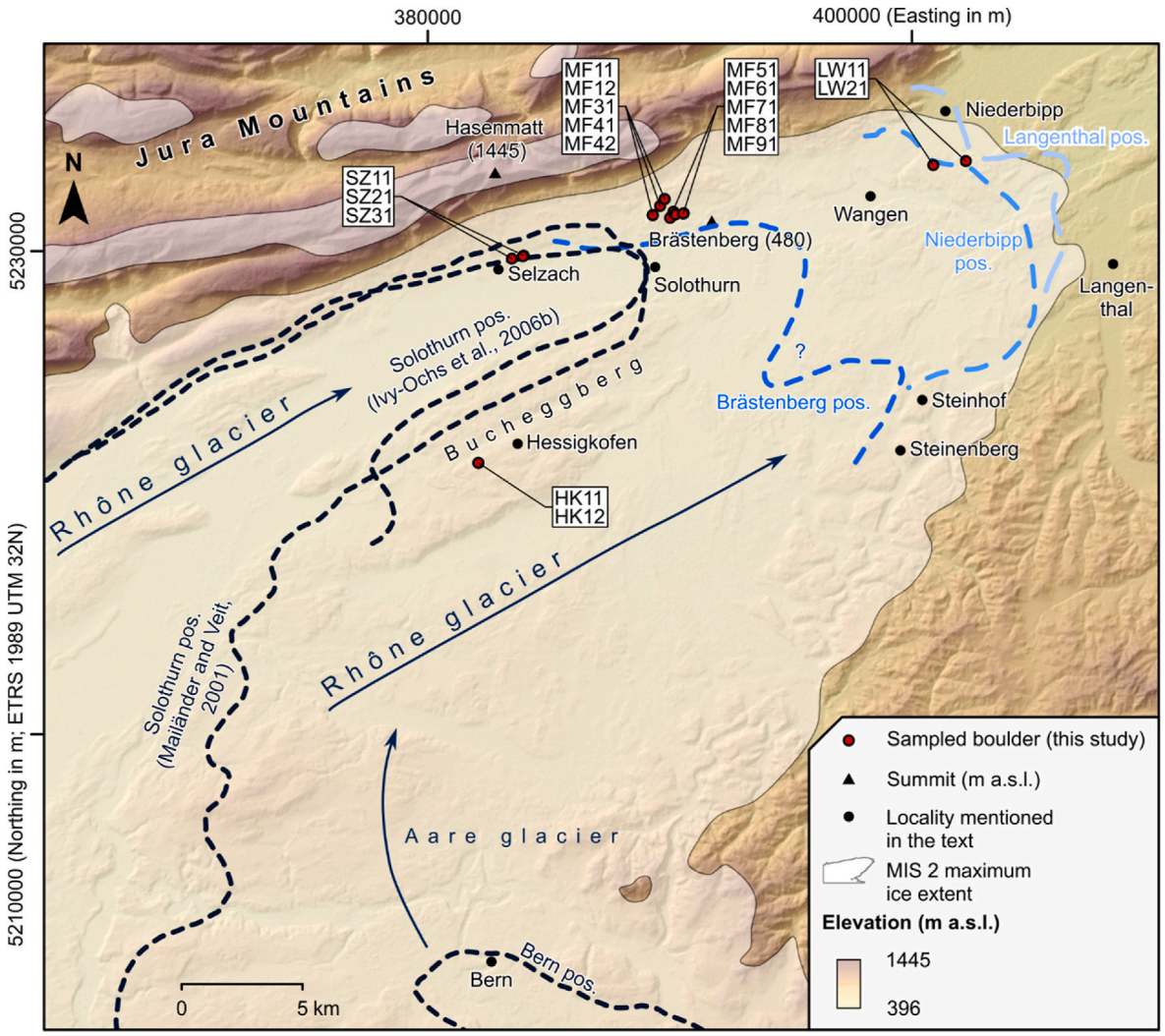

Fig. 2. Topographic map of the study area showing ice-marginal positions of the eastern lobe of the Rhône glacier and the Aare glacier, and sampling locations. For the MIS 2 maximum ice extent, see Bini et al. (2009). The Langenthal, Niederbipp, and Brästenberg positions are given in Bläsi et al. (2015). The Brästenberg position was inferred from decalcification depths in soils. See Bläsi et al. (2015) for further details. See Mailänder and Veit (2001) for the Bern position. The Solothurn position is shown in Mailänder and Veit (2001), and in Ivy-Ochs et al. (2006b). See the caption of Fig. 1 for the data source of the digital elevation model in the background.

positions, both represented by ice-marginal landforms (Bläsi et al., 2015). The maximum MIS 2 ice extent on the map of Bini et al. (2009) roughly corresponds to the Langenthal position (Fig. 2), but, as emphasised by Ivy-Ochs et al. (2021), the assumed MIS 2 maximum ice extent is not supported by geomorphological evidence.

The Brästenberg position is defined by the Brästenberg moraine complex and by moraines on the southern flank of the Jura (Nussbaum, 1951; Hantke, 1977; Laubscher et al., 2014; Bläsi et al., 2015). The moraines in the centre of Solothurn and west of the town, ascribed to the Solothurn position, document, strictly spoken, at least two different ice-marginal positions (Fig. 2; Bläsi et al., 2015). The age of the Solothurn position has been controversial and it has been suggested that the age of ice-marginal landforms may differ from their morphostratigraphic position (cf., Zimmermann, 1963, 1969; Ledermann, 1978; Ivy-Ochs et al., 2004; Bläsi et al., 2015).

Few chronological data are available on the early phase of the deglaciation of the western Swiss Plateau. The only exceptions are (i) CRE ages of four erratic boulders inside the maximum MIS 2 extent of eastern lobe of the Rhône glacier (Ivy-Ochs et al., 2004), (ii) CRE ages of erratic boulder from the Alps in the Jura and on its foothills (Graf et al., 2015), (iii) radiocarbon ages of remnants of large Late Pleistocene mammals buried in glacio-fluvial deposits (Gnägi et al., 2021, 2023), (iv) and basal radiocarbon ages from three lakes inside the MIS 2 maximum extent of the eastern lobe of the Rhône glacier [Burgäschisee (Rey et al., 2017), Moossee (Rey et al., 2020), and Lake Neuchâtel (Hadorn et al., 2002); Fig. 1]. Radiocarbon ages from the aforementioned remnants of large Pleistocene mammals in deposits (mainly glacio-fluvial) situated downstream from the assumed MIS 2 maximum position of the eastern lobe of the Rhône glacier indicate that three distinct phases of glacio-fluvial aggradation occurred between 26 and 19 ka, punctuated by phases of glacier recession (Gnägi et al., 2023). According to Gnägi et al. (2023), this points to an oscillatory behaviour of the eastern lobe of the Rhône glacier that advanced three times to a similar ice-marginal position in the region around Wangen between 26 and 19 ka. CRE ages of erratic boulders of alpine origin in the Jura and basal radiocarbon ages from lakes on the Swiss Plateau indicate that final glacier recession began at around 20—19 ka (Rey et al., 2017, 2020).

Investigating the chronology of the last deglaciation of the western Swiss Plateau in more detail is relevant for refining the knowledge of the deglaciation history of this region but is also an important reference for reconstructing atmospheric circulation patterns over Europe during the Late Pleistocene and for calibrating/validating glacier models. First, as discussed by Hofmann et al. (2020), it has been repeatedly suggested

that a meridional atmospheric circulation pattern prevailed over Europe at around 26—24 ka. At that time, humid air masses from the Mediterranean Sea probably triggered the most extensive MIS 2 advance of several glaciers to the foreland of the Alps that had their main accumulation areas south of the main weather divide in the Alps. As this was the case for the Rhône glacier (cf., Kelly et al., 2004), additional chronological data on variations in its extent could support the previous suggestion of predominant airflow from the south/south-west (e.g., Florineth and Schlüchter, 2000; Kelly et al., 2004; Kuhlemann et al., 2008; Luetscher et al., 2015; Monegato et al., 2017). Second, reconstructing the last glaciation of the western Swiss Plateau could improve glacier models. The model of Seguinot et al. (2018) probably underestimated the MIS 2 maximum extent of the eastern branch of the Rhône glacier. Additional chronological data on the spatial extent of this piedmont lobe would allow for refining the climate forcing of the model and for reconciling modelled and mapped glacier extents. Investigating the last deglaciation of the western Swiss Plateau would allow for gaining a holistic picture of glacier variations on the Swiss Plateau, thus providing additional information on potential forcings of glacier fluctuations.

For this study, we applied ^{10}Be CRE dating to geomorphologically stable and large erratic boulders to (i) infer a minimum age of the Niederbipp position, (ii) determine a minimum age for glacier recession from the Brästenberg position, (iii) obtain additional chronological constraints on the retreat of the eastern lobe of the Rhône glacier prior to the formation of the moraines of the Brästenberg position, and (iv) exposure date the moraines of the Solothurn position. Hence, this study complements previous work on the chronology of Late Pleistocene variations of the Rhône (Ivy-Ochs et al., 2004; Preusser et al., 2007; Graf et al., 2015; Gnägi et al., 2021, 2023) and Aare (Akçar et al., 2011; Wüthrich et al., 2018) glaciers. To discuss the newly obtained CRE ages in a broader context, previously published chronological data from the Swiss Plateau were recalculated.

2. Study area

The study area (Fig. 2) encompasses the western part of the Swiss Plateau and the foothills of the Jura. This region pertains to the cantons of Bern and Solothurn and was temporarily largely covered by the eastern branch of the Rhône/Aare glaciers during MIS 2.

The Jura consists of Triassic evaporites. During the Jurassic and the Cretaceous, marls and limestones were deposited on top of Triassic sedimentary rock (Institut für Geologie, Universität Bern, Bundesamt für Wasser und Geologie, 2005). Thrusting of the Jura mountains occurred as a response to the Alpine orogeny from around 10 to 3 Ma (Pfiffner, 2010). The Swiss Plateau further SE (Fig. 2) consists of Oligocene to Miocene deposits of the Lower Freshwater and the Upper Marine Molasse, i.e., sandstones, marls, and conglomerates (Pfiffner, 2010).

Unconsolidated sediments, such as till, and landforms, such as overdeepened valleys (Preusser et al., 2010; Dürst Stucki and Schlunegger, 2013; Schwenk et al., 2022; Gegg and Preusser, 2023), testify to Quaternary glaciations in this region. The hilly western Swiss Plateau encompasses several topographic highs, separated by valleys. During glaciations of the Swiss Plateau, rivers were redirected and erosion by meltwater led to the formation of the isolated Molasse bedrock highs, such as the plateau around the hamlet of Steinhof and the nearby Steinenberg (Fig. 2; Nussbaum, 1951). As pointed out by Jouvet et al. (2017), erratic boulders with lithologies occurring in the southern Valais (Arkesine, Arolla gneiss, and Allalin gabbro) and the Mont Blanc massif (Mont Blanc granites, Vallorcine conglomerate), thus originating from the southern tributary valleys of the Rhône valley in the Alps, have been identified at various localities inside the MIS 2 maximum extent of the eastern branch of the Rhône glacier. Particularly prominent erratic boulders have been identified around Steinhof and already targeted for CRE dating (Ivy-Ochs et al., 2004). Jouvet et al. (2017) proposed that enhanced precipitation over the Mont Blanc massif, and the presence of a sufficiently large and thick ice cap in the Jura were two key mechanisms that caused the diversion of erratic boulders to the eastern branch of the Rhône glacier. Moraines have been mapped at various localities in the study area (Ledermann, 1977; Gerber and Wanner, 1984; Pfirter et al., 1996; Jordi et al., 2003; Antenen et al., 2004; Laubscher et al., 2014). Examples are the Brästenberg moraine complex north-east of Solothurn (at the Brästenberg position), and the moraines on Buchegg-berg south-west of Solothurn that document the Solothurn position (Fig. 2) *sensu* Mailänder and Veit (2001), and Ivy-Ochs et al. (2006b).

After the last deglaciation, soils formed in glacial and periglacial deposits, and the western Swiss Plateau became reforested at ca. 15 ka (Veit and Gnägi, 2014). The occurrence of Holocene deposits, such as alluvial sediments, is mainly restricted to areas around today's rivers (Institut für Geologie, Universität Bern, Bundesamt für Wasser und Geologie, 2005).

3. Materials and methods

3.1. Beryllium-10 CRE dating

3.1.1. Fieldwork

Due to the removal of erratic boulders from fields and destruction of boulders on agricultural land, all sampling sites (Table 1) lay in forested areas. In total, fourteen boulders at four different sites were selected for CRE dating following established sampling strategies (e.g., Akçar et al., 2011). The sampled boulders in the Längwald area were located near the Niederbipp position. Two samples (HK11 and HK12) were obtained from an erratic boulder near the village of Hessigkofen (Fig. 3). Multiple erratic boulders were sampled at Martinsflue, a foothill of the Jura composed of Jurassic limestone. Rock samples were obtained from the MF81 and MF91 boulders on a nearby moraine of the Brästenberg position at a lower elevation (Fig. 3). The samples from the area around the village of Selzach originated from boulders on a moraine at the Solothurn position (Figs. 1 and 3).

Since only a limited number of boulders was available in the study area, not all chosen objects fulfil the proposed criteria for ideal samples. The boulders from Selzach (SZ11, SZ21 and SZ31) for example are not well-rounded and located rather at the slope than on the crest line of a moraine. Apart from these minor limitations, all boulders seemed appropriate for dating. Neither indications of intense chemical or physical weathering nor signs of toppling were observed. Between 0.5 and 1 kg of rock material from the upper 5 cm of each boulder was collected with chisel and hammer for the laboratory analysis and accelerator mass spectrometry (AMS) measurements. In three cases, a

Table 1
Location of the sampled erratic boulders, topographic shielding at sampling sites and characteristics of the rock samples.

Sample	Latitude (° WGS 1984)	Longitude (° WGS 1984)	Elevation (m a.s.l.)	Topographic shielding factor	Sample thickness (cm)
HK11	47.1339	7.4452	608	0.999976	1.5
HK12	47.1339	7.4452	608	0.999976	1.5
LW11	47.2479	7.6903	490	0.999796	4.0
LW21	47.2496	7.7080	473	0.999862	5.0
MF11	47.2274	7.5376	570	0.998647	1.0
MF12	47.2274	7.5376	570	0.998647	3.0
MF31	47.2308	7.5416	572	0.998036	3.0
MF41	47.2334	7.5439	575	0.997495	5.0
MF42	47.2334	7.5439	575	0.997495	1.5
MF51	47.2265	7.5471	498	0.998456	3.5
MF61	47.2288	7.5489	502	0.998226	4.0
MF71	47.2278	7.5499	485	0.998453	4.0
MF81	47.2283	7.5545	500	0.998866	4.0
MF91	47.2282	7.5543	500	0.998870	4.0
SZ11	47.2102	7.4612	507	0.998234	4.0
SZ21	47.2114	7.4676	502	0.998132	4.0
SZ31	47.2112	7.4672	505	0.998323	3.0

Fig. 3. Photos of the sampled erratic boulders near Hessigkofen (HK), at Martinsflue (MF), and in the vicinity of Selzach (SZ).

second sample was taken from a different part of the boulder and processed independently to verify the robustness of the methods. Geographic coordinates of the sampling sites were recorded with a handheld GPS.

3.1.2. Sample preparation and AMS measurements

Every rock sample was crushed and sieved to a grain size of 200–700 μm. After purifying quartz, Be-specific separation was undertaken following standard laboratory procedures introduced by Kohl and Nishiizumi (1992), and Ochs and Ivy-Ochs (1997). A dose of about 300 μg ^{9}Be was added to each sample. The samples were processed together with full-process blanks. The final BeO extracts were mixed with Niobium and pressed in copper target holders.

AMS measurements were performed at the 6 MV DREsden AMS facility (DREAMS) of the Helmholtz-Zentrum Dresden-Rossendorf (Akhmadaliev et al., 2013; Rugel et al., 2016) using the in-house standard SMD-Be-12 with a ^{10}Be/^{9}Be ratio of $(1.704 \pm 0.03) \times 10^{-12}$ (Akhmadaliev et al., 2013). The results of AMS measurements are traceable to the NIST 4325 standard with a ^{10}Be/^{9}Be ratio of $(2.79 \pm 0.03) \times 10^{-11}$ (Nishiizumi et al., 2007) and the ^{10}Be half-life of $(1.387 \pm 0.012) \times 10^{6}$ years (Chmeleff et al., 2010; Korschinek et al., 2010). The uncertainties of the ^{10}Be/^{9}Be ratios comprise the measurement uncertainty (counting statistics), the uncertainty of the standard (certification), and the error of the mean of the standard measurement.

3.1.3. CRE age calculations and assessment

The elevation of the sampling surfaces was retrieved from a high-resolution digital elevation model (DEM) of the study area, the SwissALTI3D with an *x*–*y* resolution of 2 m (available at https://www.swisstopo.admin.ch/de/geodata/height/alti3d.html, last access: 7 March 2023). Following the recommendations of Hofmann (2022), the high-resolution DEM of the study area was resampled to an *x*–*y* resolution of 30 m for topographic shielding factor calculations. Shielding factors were then calculated with Li's 2018 toolbox for the ArcGIS software.

Beryllium-10 CRE ages in ka before 2010 CE and internal/external uncertainties (ka) were calculated with the cosmic ray exposure program (CREp; Martin et al., 2017) available at https://crep.otelo.univ-lorraine.fr (last access: 7 September 2022). In CREp, the ^{10}Be production rate deduced from rock samples from the Chironico landslide (southern Switzerland; Claude et al., 2014) was chosen. The selected production rate was scaled to the sampling sites with time-dependent Lal/Stone scaling (Nishiizumi et al., 1989; Lal, 1991; Stone, 2000; Balco et al., 2008). As suggested by Martin et al. (2017), the ERA-40 atmosphere model (Uppala et al., 2005) was chosen in CREp. Ages were corrected for past geomagnetic activity with an atmospheric ^{10}Be-based geomagnetic

record (Muscheler et al., 2005). Age calculations were based on a ^{10}Be production rate of 4.10 ± 0.10 atoms ^{10}Be g^{-1} quartz a^{-1} at sea-level and high latitudes (SLHL). This ^{10}Be production rate concurs with the global mean ^{10}Be production rate in CREp (4.11 ± 0.19 atoms ^{10}Be g^{-1} quartz a^{-1} at SLHL). The input-sheet for CREp is given in the supplement (Table S1).

Five sampling surfaces on boulders associated with the Brästenberg position were exposure dated. Four sampling surfaces on erratic boulders beyond the Brästenberg were successfully exposure dated. Three ages were available for a moraine of the Solothurn position. Prior to averaging ages for the (i) moraine of the Solothurn position ($n = 3$), the (ii) Martinsflue area beyond the Brästenberg ice-marginal position ($n = 4$), and for the (iv) Brästenberg position ($n = 5$), a statistical assessment of the ages was undertaken following the approach of Hofmann et al. (2022): Reduced chi-squared (χ_R^2) values were computed for the three sets of ages. Reduced chi-squared statistic allowed for determining whether the variation of ages from the same landform or boulder results from analytical uncertainties ($\chi_R^2 \approx 1$) or from geomorphological factors, such as post-depositional exhumation of boulders ($\chi_R^2 \gg 1$; cf., Balco, 2011). Reduced chi-squared values were compared with a critical value from a standard χ^2-table (degree of freedom: $n - 1$; confidence interval: 95%). The critical value was then divided by the degrees of freedom. If χ_R^2 was lower than this value, the hypothesis that the data form a single population was at 95% confidence. In this case, the arithmetic mean age was computed. If χ_R turned out to be higher than the critical value, thus implying that measurement uncertainties do not fully account for the scatter in the CRE ages (cf., Balco, 2011), the age that was farthest from the average age in relation to its measurement uncertainty was considered an outlier and excluded from the dataset. This procedure was repeated until the remaining ages yielded an acceptable χ_R value. If there were less than three ages, the procedure was stopped. The uncertainties of the average ages were determined by adding the mean internal uncertainty of the ages and the error of the ^{10}Be production rate in quadrature (e.g., Le Roy et al., 2017; Braumann et al., 2020; Hofmann et al., 2022).

3.2. Recalculation of previously published ^{10}Be CRE ages

Fifty-nine previously published ages for the regions formerly covered by the (i) eastern branch of the Rhône glacier (Ivy-Ochs et al., 2004; Graf et al., 2015), (ii) the Aare glacier (Akçar et al., 2011; Wüthrich et al., 2018), and (iii) the Reuss glacier (Reber et al., 2014; Kamleitner et al., 2023) were recalculated with CREp. See Fig. 1 for the location of these regions. To ensure consistency, the parameters listed above were chosen in CREp. ^{10}Be concentrations in Ivy-Ochs et al. (2004) were determined with the S555 standardisation. As CREp requires ^{10}Be concentrations determined with the 07KNSTD standardisation, ^{10}Be concentrations in Ivy-Ochs et al. (2004) were recalculated with a conversion factor from Balco (2016). Ages were excluded, as done in the original publications. Mean ages and associated uncertainties were calculated as outlined in Sect. 3.1.3. The input-sheet for CREp is given in the supplement (Table S2).

3.3. Recalibration of radiocarbon ages

Published basal radiocarbon ages of lakes inside the maximum MIS 2 extent of the eastern lobe of the Rhône glacier were recalibrated with the OxCal software (version 4.4; Bronk Ramsey, 2009) and IntCal20 (Reimer et al., 2020). They are expressed by the 95% interval of calibration (Millard, 2014). To ensure comparability with newly acquired and recalculated CRE ages, calibrated ages were converted in ka (kiloyears before 2010 CE).

4. Results

See Table 2 for the results of the AMS measurements and the CRE ages. The location of the sampled boulders at the four sampling localities, Martinsflue, Hessigkofen, Längwald, and Selzach, and their CRE ages are shown in Fig. 4.

4.1. Längwald

Due to low ^{9}Be currents during AMS measurements (dropping from 0.4 to 0.1 μA during the first 15 s of AMS measurements), the ^{10}Be concentration in the sample from the LW-11 erratic boulder at the Niederbipp position should not be regarded as reliable and, thus, no age was computed. The LW21 erratic boulder gave an age of 19.1 ± 0.7 ka (Fig. 4).

4.2. Martinsflue

As can be seen in Fig. 4, a chain of hills is situated in the area north-west of the Brästenberg position. The hills are composed of Jurrassic limestone and belong to the Sankt-Verena fault-bend fold that is delimited to the north-west by a fault, the Martinsflue fault (Fig. 4; Bläsi et al., 2015). Numerous erratic boulders, i.e., glacially transported granites from the Aare and/or Mont Blanc massif in the Alps, directly rest on their surface. Three of them were sampled for this study.

The MF11 sampling surface on an erratic boulder at an elevation of 570 m a.s.l. gave an age of 16.8 ± 0.8 ka. Due to relatively low ^{10}Be counts ($n = 185$) and a rapid decrease of ^{9}Be currents from 1 to 0.1 μA during AMS measurements, the ^{10}Be concentration in the sample from the MF12 sampling surface on the same boulder should not be considered reliable. Therefore, we did not compute an age of the sampling surface. The MF31 boulder at an elevation of 572 m a.s.l. further north-east gave an age of 17.8 ± 0.8 ka. Two rock samples were obtained from another erratic boulder at an elevation of 575 m a.s.l. further north-east. The MF41 and MF42 sampling surfaces yielded overlapping ages of 16.8 ± 1.0 ka and 16.2 ± 0.9 ka, respectively. A χ_R^2 value of 0.8 was computed for the MF11, MF31, MF41 and MF42 sampling surfaces, thus indicating that measurement uncertainties account for the variation in ages. Hence, the boulders outboard the Brästenberg position gave a mean age of 16.9 ± 0.9 ka.

Fig. 4c reveals that several hills and ridges are situated in the area south-east of Martinsflue. The Brästenberg hill and another mound further west feature an undulating and smooth surface. A roughly west-east trending depression separates the mound west of Brästenberg from an elongated ridge further north. The elongated ridge north of the depression has a sharp crest and is interpreted as a moraine. Numerous erratic boulders, i.e., glacially transported granites from the Aare and/or Mont Blanc massif in the Alps, are situated on its surface. Brästenberg, the mound further west and the sharp-crested moraine constitute a moraine complex indicative of the Brästenberg position (Bläsi et al., 2015).

The sampled MF81 and MF91 erratic boulders were situated near the crest of the sharp-crested moraine at 500 m a.s.l. and gave ages of 18.8 ± 0.9 ka and 21.8 ± 1.7 ka, respectively. Three erratic boulders, the MF51, MF61 and MF71 boulders, were sampled in the area west of the sharp-crested ridge. The MF51 and MF71 boulders lay at an elevation of 498 and 485 m a.s.l., respectively, and are associated with the Brästenberg ice-marginal position. The boulders yielded ages of 30.9 ± 1.5 ka and 20.0 ± 1.1 ka, respectively. The MF61 boulder further north (at 502 m a.s.l.) may be also associated with the Brästenberg position and gave an age of 25.6 ± 1.5 ka. A reduced chi-squared value of 8.9 was computed for the boulders unambiguously associated with the Brästenberg position (MF51, MF71, MF81, and MF91 boulders). This value exceeded the critical value from the χ^2-table. The ages of the MF51 and MF81 boulders were farthest from the average age in relation to their measurement uncertainties and were therefore considered outliers.

Table 2
^{10}Be concentrations in the samples and ages of the erratic boulders near Hessigkofen (HK), in the Längwald area (LW), at Martinsflue (MF), and in the vicinity of Selzach (SZ).

Sample	Quartz (g)	Carrier solution added (mg)	Beryllium-10/ Beryllium-9 ($\times 10^{-14}$)	Beryllium-10 concentration (atoms g^{-1} quartz)	Beryllium-10 concentration uncertainty (atoms g^{-1} quartz)	CRE age and external (internal) uncertainty (ka)
HK11	18.22	357.2[a]	10.64 ± 0.49	129400[c]	6700[c]	18.9 ± 1.0 (0.9)
HK12	20.82	356.6[a]	12.38 ± 0.52	132900[c]	6200[c]	19.4 ± 1.0 (0.9)
LW11	36.00	159.2[b]	13.2 ± 3.9	87000[d,e]	26000[d,e]	–[e]
LW21	22.09	156.7[b]	10.71 ± 0.30	113000[d]	3400[d]	19.1 ± 0.7 (0.6)
MF11	24.30	354.3[a]	12.22 ± 0.46	111500[c]	4700[c]	16.8 ± 0.8 (0.7)
MF12	25.52	294.0[a]	20.7 ± 3.9	153100[f,g]	30000[f,g]	–[g]
MF31	19.90	359.3[a]	10.41 ± 0.38	116400[c]	4900[c]	17.8 ± 0.8 (0.7)
MF41	11.17	347.6[a]	5.97 ± 0.28	107800[c]	6300[c]	16.8 ± 1.0 (1.0)
MF42	31.70	356.5[a]	15.06 ± 0.68	107400[c]	5300[c]	16.2 ± 0.9 (0.8)
MF51	8.49	349.6[a]	7.60 ± 0.24	189600[h]	7600[h]	30.9 ± 1.5 (1.3)
MF61	15.08	344.7[a]	10.81 ± 0.55	156800[j]	8900[j]	25.6 ± 1.5 (1.4)
MF71	11.64	355.7[a]	6.47 ± 0.29	120500[k]	6400[k]	20.0 ± 1.1 (1.0)
MF81	10.14	341.8[a]	5.79 ± 0.19	114000[h]	4500[h]	18.7 ± 0.8 (0.7)
MF91	5.44	347.2[a]	3.71 ± 0.21	133000[k]	10000[k]	21.8 ± 1.7 (1.6)
SZ11	26.54	346.4[a]	28.8 ± 1.3	246000[j]	11000[j]	40.1 ± 2.0 (1.8)
SZ21	14.65	349.7[a]	2.01 ± 0.19	23400[j]	4000[j]	4.0 ± 0.7 (0.7)
SZ31	8.15	352.0[a]	18.91 ± 0.54	525000[h]	16000[h]	86.1 ± 3.3 (2.6)

[a] Beryllium-9 concentration: 1000.0 ± 8.0 μg/g.
[b] Beryllium-9 concentration: 2246 ± 11 μg/g (Merchel et al., 2013).
[c] The Be-10 concentrations and associated uncertainties were corrected with a batch-specific chemical blank [Beryllium-10/Beryllium-9 ratio: (7.8 ± 1.1) × 10^{-15}; carrier added: 350.0 mg].
[d] The Be-10 concentrations and associated uncertainties were corrected with a batch-specific chemical blank [Beryllium-10/Beryllium-9 ratio: (9.9 ± 2.5) × 10^{-16}; carrier added: 154.7 mg].
[e] Due to low ^{9}Be currents during AMS measurements (dropping from 0.4 to 0.1 μA during the first 15 s of AMS measurements), the ^{10}Be concentration in the sample from the LW-11 erratic boulder at the Niederbipp position should not be regarded as reliable.
[f] The Be-10 concentration and the associated uncertainty were corrected with a batch-specific chemical blank [Beryllium-10/^{9}Be ratio: (7.96 ± 0.75) × 10^{-15}; carrier added: 300.0 mg].
[g] Due to relatively low ^{10}Be counts ($n = 185$) and a rapid decrease of ^{9}Be currents from 1 to 0.1 μA during AMS measurements, the ^{10}Be concentration in the sample from the MF12 sampling surface should not be considered reliable.
[h] The Be-10 concentrations and associated uncertainties were corrected with a batch-specific chemical blank [Beryllium-10/Beryllium-9 ratio: (7.1 ± 1.2) × 10^{-15}; carrier added: 350.9 mg].
[j] The Be-10 concentrations and associated uncertainties were corrected with a batch-specific chemical blank [Beryllium-10/Beryllium-9 ratio: (5.4 ± 1.6) × 10^{-15}; carrier added: 349.8 mg].
[k] The Be-10 concentrations and associated uncertainties were corrected with a batch-specific chemical blank [Beryllium-10/Beryllium-9 ratio: (5.7 ± 1.0) × 10^{-16}; carrier added: 356.1 mg].

The remaining ages gave a mean age of 20.2 ± 1.2 ka.

4.3. Hessigkofen

The HK11 and HK12 sampling surfaces on the erratic boulder sampled near Hessigkofen gave ages of 18.9 ± 1.0 ka and 19.4 ± 1.0 ka, respectively. An arithmetic mean age of 19.2 ± 1.0 ka was calculated for this boulder.

4.4. Selzach

The SZ11, SZ21 and SZ31 boulders on a moraine of the Solothurn position yielded scattering ages (41.1 ± 2.0 ka, 4.1 ± 0.6 ka, and 86.1 ± 3.3 ka, respectively). Due to the large scatter, no landform age was computed (Fig. 4b).

5. Discussion

5.1. Significance of the newly acquired CRE ages

The presented ages were not corrected for postglacial weathering and denudation. Ivy-Ochs et al. (2004) inferred a denudation rate of 3 mm ka^{-1} for the erratic boulders in the Steinhof Area. Assuming this constant erosion rate during CRE age calculations resulted in an average ageing of 6.5%. The age for the SZ31 boulder shifted by 28% with respect to the uncorrected age. For most boulders, the age shift was in the order of a few centuries and, therefore, the uncorrected ages might be slightly underestimated.

The LW21 boulder lay at the Niederbipp position. The age of the boulder (19.1 ± 0.7 ka) overlaps with the average age of the boulders at the Brästenberg position upstream from the Niederbipp position (20.2 ± 1.2 ka). The age of the LW21 boulder is older than the mean age of the erratic boulders at Martinsflue, outboard the Brästenberg position (16.9 ± 0.9 ka). We therefore interpret the age of the LW21 boulder as a minimum age of the Niederbipp position.

The MF11, MF31, MF41 and MF42 sampling surfaces at Martinsflue were situated on boulders at much higher elevations (570–575 m a.s.l.) than those at the Brästenberg position. Therefore, the deglaciation of this area must have occurred earlier than the deposition of the erratic boulders at the Brästenberg position and moraine formation. The apparent minimum age for ice recession from the Brästenberg position (20.2 ± 1.2 ka) conflicts with the mean age (16.9 ± 0.9 ka) of the boulders outboard this ice-marginal position. We propose that either (i) the mean age of the MF11, MF31, MF41, and MF42 sampling surfaces underestimates the deglaciation age of the Martinsflue area outboard the Brästenberg position (i.e., the mean age of the erratic boulders associated with the Brästenberg position should be interpreted as minimum age for glacier recession from the ice-marginal position) or (ii) the erratic boulders at the Brästenberg position experienced pre-exposure to cosmic-rays (i.e., the mean age of the erratic boulders beyond the Brästenberg position should be interpreted as the appropriate minimum age for glacier recession from this ice-marginal position).

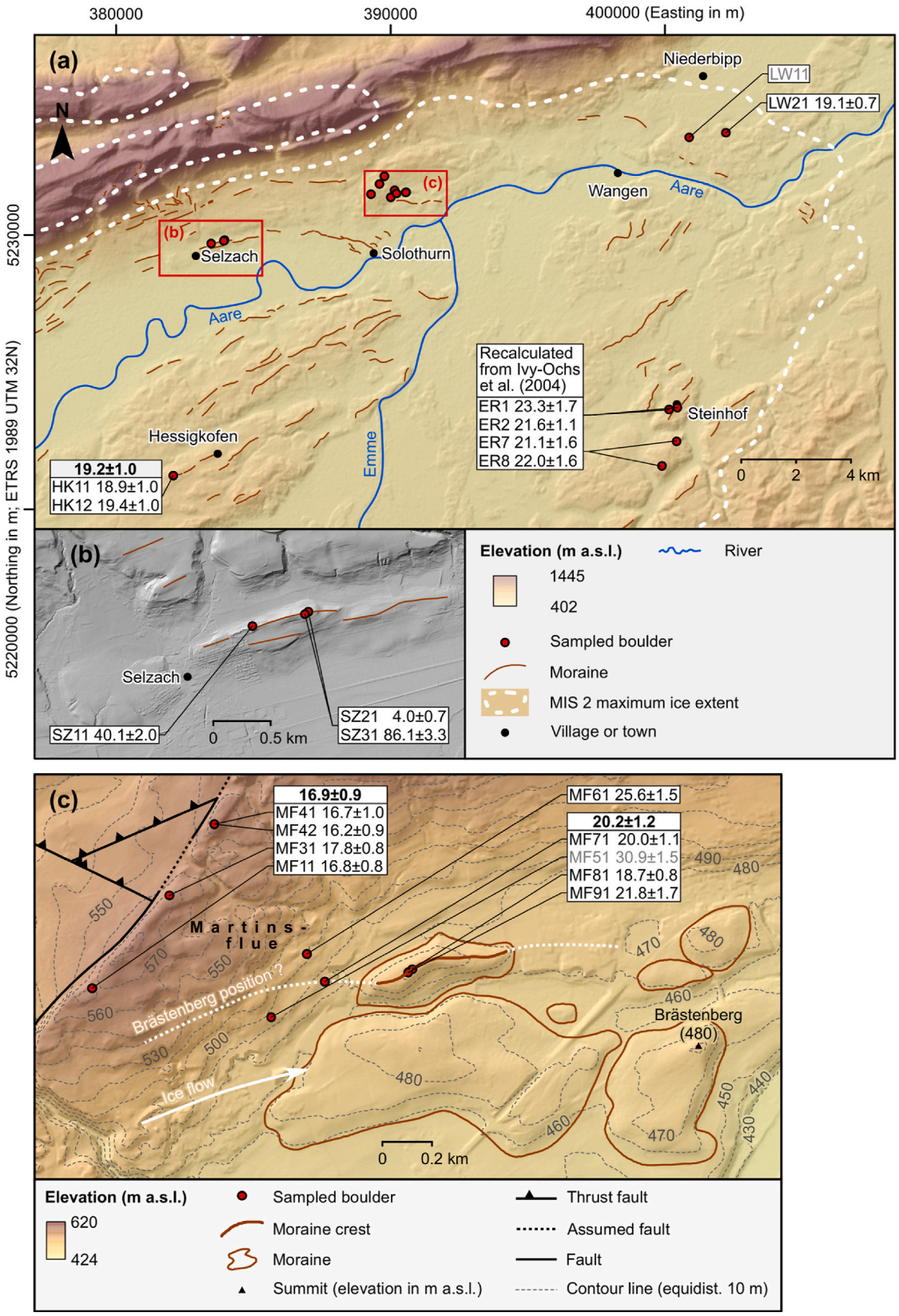

Fig. 4. (a) Topographic map of the region around Solothurn showing the MIS 2 maximum ice extent (Bini et al., 2009), moraines (Ledermann, 1977; Gerber and Wanner, 1984; Pfirter et al., 1996; Jordi et al., 2003; Antenen et al., 2004; Laubscher et al., 2014), sampled boulders, and CRE ages of sampled boulders. For the source of the elevation data in the background, see the caption of Fig. 1. (b) Moraines at the Solothurn position in the vicinity of Selzach and sampled boulders. The hillshade in the background was derived from the SwissALTI3D (available at https://www.swisstopo.admin.ch/de/geodata/height/alti3d.html, last access: 6 September 2022). (c) Topographical/geomorphological map of the area around Martinsflue and Brästenberg. The DEM in the background is the SwissALTI3D. Thrust faults, assumed faults, and faults according to Laubscher et al. (2014). All ages of erratic boulders and associated external uncertainties are expressed in ka (kiloyears before 2010 CE) and ka, respectively. Ages in grey were excluded. Bold ages are landform ages. © BFS, ThemaKart 2022 for rivers.

The MF41 and MF42 sampling surfaces were situated on an exceptionally large erratic boulder that directly rested on a small plateau composed of Jurassic limestone (Fig. 3). Therefore, it is rather unlikely that the boulder toppled or rotated after deglaciation. This is also true for the boulder from which we obtained the MF11 sample (Fig. 3). Therefore, two conceivable explanations for the first scenario ages are postglacial weathering of the sampled rock surfaces or post-depositional exhumation of the sampling surfaces (cf., Ivy-Ochs et al., 2007). Due to the internal robustness of the ages of the sampling surfaces on erratic boulders beyond the Brästenberg position ($\chi_R^2 = 0.8$), we deem the first explanation rather unlikely. On the other hand, due to the limited number of CRE ages ($n = 4$) for this area, it is possible that the ages just agree by chance. The second explanation would imply that glacial sediments around the boulders must have been affected by erosion and washed away. Given that the sampled boulders were large (Fig. 3), significant amounts of sediments must have been removed from the area around the boulders. Previous work (Wüthrich et al., 2017) concluded that, at Steinhof (Fig. 2), about 120 cm of the till of the last glaciation have been eroded. This total denudation is based on a deglaciation age of ~24 ka and a denudation rate of 6 cm ka^{-1} (Wüthrich et al., 2017). Therefore, it appears possible that glacial sediments around the sampled boulders may have been removed after the deglaciation.

According to the second scenario, the boulders at the Brästenberg position, including those on the moraine (MF81 and MF91), experienced pre-exposure to cosmic rays and the consistent ages of erratic boulders beyond the Brästenberg position reflect the timing of the onset of glacier retreat from this ice-marginal position. This scenario is supported by the observation that complex exposure histories seem to be prevalent in the area formerly occupied by the eastern branch of the Rhône glacier. Indeed, Graf et al. (2015) obtained an unrealistically old CRE age when exposure dating the RH-03c erratic boulder on Bözingenberg, a foothill of the Jura WSW of the Martinsflue area. Although the boulder was located clearly inside the MIS 2 extent of the eastern lobe of the Rhône glacier (see Bini et al., 2009), Graf et al. (2015) obtained a (recalculated) age of 56.4 ± 3.9 ka. In general, apparently "too-old" ages stem from pre-exposure to cosmic radiation when older glacial deposits are reworked or when boulders originating from previously exposed bedrock fall onto glaciers (Ivy-Ochs et al., 2007; Ivy-Ochs and Kober, 2008). Limited glacial erosion has also been proposed as explanation for apparently "too-old" ages (Ruszkiczay-Rüdiger et al., 2021) and may result from the presence of cold-based ice that allows for the preservation of formerly existing landforms. A well-known example for a relict landscape is the former centre of the Fennoscandian ice sheet where pre-existing landforms have been preserved due to cold-based ice and limited glacial erosion (e.g., Stroeven et al., 2002). It has been suggested that not only this ice sheet, but also the piedmont glaciers in the Swiss Plateau might have been predominantly cold-based (Haeberli and Schlüchter, 1987; Haeberli, 2005).

Three explanations are proposed for the possible pre-exposure of the sampled boulders at the Brästenberg position. First, the boulders were already exposed to cosmic rays in the Alps, fell onto the Rhône or Aare glacier and were supraglacially transported to their present location. Second, the boulders were glacially transported to some location inside the MIS 2 maximum extent of the eastern lobe of the Rhône glacier, exposed to cosmic radiation, picked up by the eastern lobe of the Rhône glacier, and eventually deposited at their present location. Third, the boulders were exposed to cosmic rays, remained in their original position during the MIS 2 maximum advance of the eastern lobe of the Rhône glacier, were affected by limited subglacial erosion, and became finally exposed to cosmic rays during the last deglaciation. The sampled moraine at the Brästenberg position has a sharp crest. Thus, it is unlikely that the Rhône glacier overprinted this landform during a re-advance. Therefore, the limited glacial erosion hypothesis would only be appropriate for the MF51 and MF71 erratic boulders west of the moraine.

To understand the significance of the ages of boulders beyond the Brästenberg position, it is necessary to rule out that the boulders at this ice-marginal position were affected by pre-exposure to cosmic rays. Due to limited laboratory capacities, we were unable to determine the concentration of cosmogenic ^{14}C in the rock samples which could have potentially helped us to rule out complex exposure histories (see Wirsig et al., 2016b or Hippe, 2017 for further methodological details). Carbon-14 CRE dating of these boulders would, however, only work if the MF51, MF71, MF81, and MF91 boulders were either sufficiently long covered by ice or affected by glacial erosion to reset the ^{14}C inventory of the boulders' surface.

As we deem the scenario unlikely that the sampled boulders at the Brästenberg position were affected by pre-exposure to cosmic rays and that none of the sampled boulders beyond this ice-marginal position experienced pre-exposure to cosmic rays, our preferred scenario is that glacier recession from the Brästenberg position began no later than 20.2 ± 1.2 ka. Nevertheless, it is also possible that the mean age of the sampling surfaces on erratic boulders outboard this ice-marginal position (16.9 ± 0.9 ka) is closer to the true age of the onset of glacier recession from this ice-marginal position. With its numerous large erratic boulders, Martinsflue is a key area for understanding the chronology of the retreat of the eastern lobe of the Rhône glacier. Therefore, this area warrants further investigation.

The overlapping ages of the sampling surfaces on the erratic boulder near Hessigkofen are internally consistent and indicate that the area around Hessigkofen became deglaciated no later than 19.2 ± 1.0 ka. Thus, deglaciation may have occurred at the same time as the formation of the sampled moraine of the Brästenberg position.

With 4.0 ± 0.7 ka to 86.1 ± 3.3 ka, the CRE ages of boulders on a moraine near the village of Selzach scatter strongly. We attribute the CRE age of the SZ21 boulder (4.0 ± 0.7 ka) to post-depositional exhumation. The moraine near Selzach lies clearly inside the MIS 2 extent of the eastern lobe of the Rhône glacier (see Bini et al., 2009). The ages of the SZ11 (40.1 ± 2.0 ka) and SZ31 (86.1 ± 3.3 ka) boulders appear to be unrealistically old. This probably again results from pre-exposure before moraine formation and/or limited glacial erosion. It is also possible that the sampled moraine near Selzach is a landform of pre-MIS 2 age and that it was overridden by the eastern lobe of the Rhône glacier during the most extensive MIS 2 advance.

5.2. *Towards a chronology of last deglaciation of the region formerly occupied by the eastern lobe of the Rhône glacier*

Together with recalculated CRE ages of erratic boulders from various localities on the Swiss Plateau and in the Jura (Table 3 & Fig. 5), and recalibrated radiocarbon ages (Table 4), the newly obtained CRE ages (Table 2 & Fig. 4) allow for reconstructing the chronology of the retreat of the eastern lobe of the Rhône glacier in more detail.

As previously discussed (e.g., Veit and Gnägi, 2014), the location of the MIS 2 maximum ice-marginal position of the eastern lobe of the Rhône glacier in the area around Wangen remains largely elusive. Ivy-Ochs et al. (2021: p. 281) noted that the eastern lobe of the Rhône glacier 'remained in the region of Wangen for several thousand years, oscillating at various positions'. However, as landforms at the Langenthal position have not been numerically dated (Fig. 2; Bläsi et al., 2015), it remains unclear whether this position is of MIS 2 age. Gnägi et al. (2023) radiocarbon dated remnants of large Pleistocene mammals buried in glacio-fluvial deposits downstream of the assumed MIS 2 maximum extent of the eastern lobe of the Rhône glacier, including woolly rhinoceros (*Coelodonta antiquitatis*), woolly mammoth (*Mammuthus primigenius*), and Alpine ibex (*Capra ibex*) remains. They concluded that three distinct sub-phases of glacio-fluvial aggradation downstream from its assumed MIS 2 maximum position occurred in the period between ca. 26 and 20 ka. According to Gnägi et al. (2023), the most recent phase of glacio-fluvial aggradation lasted until ca. 20 ka.

This age appears to conflict with (recalculated) CRE ages of erratic boulders around Steinhof and on Steinenberg, ranging from 23.3 ± 1.7 ka to 21.1 ± 1.6 ka (Ivy-Ochs et al., 2004). However, we argue that the

Table 3
Recalculated ^{10}Be CRE ages from boulders at key localities on the Swiss Plateau. Italic ages were excluded in the original publications.

Locality	Landform	Landform age (ka)	Boulder	Originally reported cosmic-ray exposure age and external uncertainty (ka)	Recalculated ^{10}Be cosmic-ray exposure age and external uncertainty (internal uncertainty; ka)	Reference
Jura Mountains	Erratic boulders at Montoz and Bözingenberg	–	MO-04-01	129.7 ± 8.6 (4.7)	116.6 ± 4.4 (3.4)	Graf et al. (2015)
			MO-04-02	95.0 ± 12.0 (11.1)	88.1 ± 9.2 (8.9)	
			MO-04-03	76.4 ± 5.4 (6.6)	71.8 ± 4.8 (4.5)	
			MO-04-04	143.2 ± 11.4 (8.2)	127.4 ± 6.7 (6.0)	
			RH-2	*15.9 ± 1.1 (0.8)*	*15.6 ± 0.9 (0.8)*	
			RH-3c	59.1 ± 5.2 (4.2)	56.4 ± 3.9 (3.7)	
	Erratic boulders near the town of Neuchâtel	–	PAB-1	21.4 ± 1.7 (1.3)	20.9 ± 1.3 (1.2)	
			PAB-2	22.4 ± 1.6 (1.2)	21.8 ± 1.2 (1.1)	
			VDR-1	*31.8 ± 3.9 (2.6)*	*30.9 ± 2.6 (2.5)*	
			VDR-2	20.2 ± 1.8 (1.4)	19.8 ± 1.4 (1.3)	
			VDR-3	*43.6 ± 3.0 (2.1)*	*42.0 ± 2.1 (1.8)*	
			VDR-4	26.7 ± 2.3 (1.9)	26.1 ± 1.9 (1.8)	
			MDA-1	144.0 ± 9.6 (5.3)	127.8 ± 4.9 (3.8)	
			GRI-1	22.6 ± 1.7 (1.3)	22.1 ± 1.3 (1.2)	
			COR-1	50.0 ± 3.4 (2.3)	47.9 ± 2.5 (2.1)	
	Erratic boulders around le Suchet	–	PBOL-1	21.0 ± 1.7 (1.3)	20.5 ± 1.3 (1.2)	
			CREB-1	20.1 ± 1.4 (1.1)	19.7 ± 1.1 (1.0)	
			CREB-2	15.5 ± 1.4 (1.2)	15.2 ± 1.1 (1.1)	
			CREB-3	17.7 ± 1.4 (1.1)	17.4 ± 1.1 (1.0)	
			PEB-1	34.8 ± 2.5 (1.9)	33.8 ± 1.9 (1.7)	
			GJ-1	19.9 ± 1.6 (1.2)	19.5 ± 1.2 (1.1)	
			GJ-2	39.0 ± 3.6 (3.1)	37.8 ± 2.8 (2.7)	
Aare valley	Erratic boulders in the surroundings of Steinhof	–	ER1	18.9 ± 1.5 [b]	23.3 ± 1.7 (1.6)	Ivy-Ochs et al. (2004)
			ER2	19.4 ± 1.3 [b]	21.6 ± 1.1 (1.0)	
			ER7	*15.8 ± 1.3* [b]	*21.1 ± 1.6 (1.6)*	
			ER8	17.9 ± 1.4 [b]	22.0 ± 1.6 (1.5)	
	Erratic boulders at Möschberg	–	MOE-1	*13.6 ± 1.2 (0.5)*	*15.3 ± 0.6 (0.5)*	Akçar et al. (2011)
			MOE-2	18.1 ± 0.8 (1.7)	20.3 ± 1.0 (0.9)	
			MOE-3	*7.5 ± 0.7 (0.4)*	*8.5 ± 0.4 (0.4)*	
	Moraines at the Gurten position	18.9 ± 1.0	GS1	20.7 ± 2.2 [b]	19.9 ± 1.6 (1.6)	Wüthrich et al. (2018)
			GS2	*7.8 ± 0.6* [b]	*7.7 ± 0.3 (0.2)*	
			GS3	19.8 ± 1.7 [b]	19.1 ± 1.0 (0.8)	
			GS4	*13.0 ± 1.0* [b]	*13.0 ± 0.5 (0.3)*	
			GS5	18.2 ± 1.5 [b]	17.5 ± 0.6 (0.4)	
	Moraines at the Bern position	17.0 ± 0.8	BS1	*9.0 ± 1.0* [b]	*8.3 ± 0.6 (0.6)*	
			BS2	19.0 ± 2.0 [b]	18.3 ± 1.4 (1.3)	
			BS3	16.7 ± 1.5 [b]	15.9 ± 0.8 (0.7)	
			BS4	15.6 ± 1.3 [b]	14.9 ± 0.6 (0.4)	
			BS5	18.4 ± 1.5 [b]	17.6 ± 0.6 (0.5)	
			BS6	18.7 ± 1.4 [b]	18.2 ± 0.6 (0.5)	
Reuss valley	Erratic boulders at the Untertannwald ice-marginal position	21.3 ± 1.0	Reuss-21	22.0 ± 0.9 (1.4) [c]	21.5 ± 1.0 (0.8)	Reber et al. (2014)
			Reuss-22	22.2 ± 1.0 (1.5) [c]	21.7 ± 1.1 (0.9)	

(*continued on next page*)

Table 3 (*continued*)

Locality	Landform	Landform age (ka)	Boulder	Originally reported cosmic-ray exposure age and external uncertainty (ka)		Recalculated ^{10}Be cosmic-ray exposure age and external uncertainty (internal uncertainty; ka)	Reference
			Reuss30	21.2 ± 1.4 (0.9)	[c]	20.6 ± 1.0 (0.8)	Kamleitner et al. (2023)
			Reuss31	*15.2 ± 1.0 (0.7)*	[c]	*15.0 ± 0.8 (0.7)*	
			Reuss45	*18.3 ± 1.4 (1.0)*	[c]	*17.9 ± 1.0 (1.0)*	
			Reuss46	21.7 ± 1.6 (1.2)	[c]	21.1 ± 1.2 (1.1)	
	Erratic boulders on the Wagenrain Molasse ridge	–	Reuss40	20.3 ± 1.6 (1.3)	[c]	19.8 ± 1.3 (1.2)	
			Reuss41	17.4 ± 1.3 (1.0)	[c]	17.1 ± 1.0 (0.9)	
			Reuss42	17.2 ± 1.3 (1.0)	[c]	16.9 ± 1.0 (0.9)	
	Erratic boulders at the Mellingen ice-marginal position	19.0 ± 1.0	Reuss32	21.1 ± 1.4 (1.4)	[c]	20.6 ± 1.0 (0.9)	
			Reuss33	*53.6 ± 3.4 (2.0)*	[c]	*50.8 ± 2.3 (1.9)*	
			Reuss34	18.6 ± 1.2 (0.8)	[c]	18.2 ± 0.9 (0.8)	
			Reuss35	19.1 ± 1.2 (0.8)	[c]	18.7 ± 0.8 (0.7)	
			Reuss36	20.5 ± 1.3 (0.8)	[c]	20.0 ± 0.9 (0.8)	
			Reuss37	*14.1 ± 1.0 (0.8)*	[c]	*14.0 ± 0.8 (0.7)*	
			Reuss38	17.7 ± 1.3 (1.0)	[c]	17.3 ± 1.0 (0.9)	
			Reuss44	20.0 ± 1.8 (1.6)	[c]	19.6 ± 1.5 (1.4)	
	Erratic boulders at the Stetten ice-marginal position	19.2 ± 1.1	Reuss39	20.8 ± 1.7 (1.3)	[c]	20.2 ± 1.3 (1.2)	
			Reuss-20	18.6 ± 1.3 (0.9)	[c]	18.3 ± 1.0 (0.9)	Reber et al. (2014)

[a] Internal uncertainties (ka) in parentheses.
[b] Ivy-Ochs et al. (2004) and Wüthrich et al. (2018) did not report internal uncertainties.
[c] Reber et al. (2014) and Kamleitner et al. (2023) only reported CRE ages corrected for denudation (assumed denudation rate: 1 mm/ka).

area around Steinhof and Steinenberg remained ice-free during the most recent period of glacio-fluvial aggradation (until ~20 ka). Variations in ice thickness during the different advances of the eastern lobe of the Rhône glacier could, apart from the time lag between deglaciation and the deposition of macrofossils, explain the offset between the (recalculated) CRE ages for the Steinhof area/Steinenberg and the (recalibrated) basal radiocarbon age of the nearby Burgäschisee (18.9—18.4 ka; Rey et al., 2017). The minimum age of the Niederbipp position (19.1 ± 0.7 ka) supports the hypothesis of Gnägi et al. (2023) that glacio-fluvial aggradation lasted until ~20 ka downstream from the front of the eastern branch of the Rhône glacier.

The beginning of ice decay in the Jura after the MIS 2 maximum advance of the Rhône glacier is constrained by (recalculated) CRE ages of erratic boulders from the Alps. The area at an elevation of about 1250 m a.s.l. around Le Chasseron in the Jura, where Graf et al. (2015) sampled the CREB-1, CREB-2, and CREB-3 erratic boulders, was abandoned by the eastern lobe of the Rhône glacier no later than 19.7 ± 1.1 ka. This minimum age for deglaciation corresponds to the (recalculated) deglaciation age (20.5 ± 1.3 ka) for the nearby area around the PBOL-1 erratic boulder. According to the CRE age of the VDR-2 erratic boulder, the ice retreated from Val de Ruz near the town of Neuchâtel (about 40 km further NE) by 19.8 ± 1.4 ka at the latest. The RH-2 and RH-3c boulders on Bözingenberg, a foothill of the Jura further NE, gave (recalculated) CRE ages of 15.6 ± 0.9 ka and 56.4 ± 3.9 ka, respectively.

Graf et al. (2015) attributed the age of the RH-2 boulder to post-depositional exhumation, whereas the SH-3c boulder was probably repositioned by the eastern lobe of the Rhône glacier during its maximum MIS 2 advance. Therefore, the timing of deglaciation of this area remains unknown. Overall, the ages for the Jura are consistent with the hypothesis of Gnägi et al. (2023) that final glacier retreat on the western Swiss Plateau began at around 20 ka.

Moraines at the Brästenberg and Solothurn positions indicate repeated phases of ice-marginal stability during the last deglaciation of the western Swiss Plateau (Fig. 2; Nussbaum, 1951; Hantke, 1977; Ledermann, 1978; Bläsi et al., 2015). According to our preferred interpretation, the eastern lobe of the Rhône glacier receded from the moraines of the Brästenberg position no later than 20.2 ± 1.2 ka. This interpretation is supported by the (recalibrated) basal radiocarbon age of both Burgäschisee (18.9—18.4 ka; Rey et al., 2017) and Moossee (19.6—19.0 ka; Rey et al., 2020) 20 km further south-west (Fig. 1). Due to the uncertainties associated with CRE dating, it is not possible to evaluate whether the area around Hessigkofen was already ice-free during the formation of the moraines at the Brästenberg position. The position of the ice margin of the eastern lobe of the Rhône glacier remains largely elusive. The ice extent shown in Fig. 2 was inferred from decalcification depths in soils (Bläsi et al., 2015). Ledermann (1978) assumed that the ice extent was more restricted and ascribed moraines on Bucheggberg (Fig. 2) to the Brästenberg position.

CRE dating of erratic boulders on a moraine of the Solothurn position did not prove to be successful. Hence, the timing of the onset of glacier recession from the moraines of this ice-marginal position could not be constrained. Nevertheless, the newly acquired CRE ages of erratic boulders associated with the Brästenberg position and the recalibrated basal radiocarbon age from Lake Neuchâtel (recalibrated from Hadorn

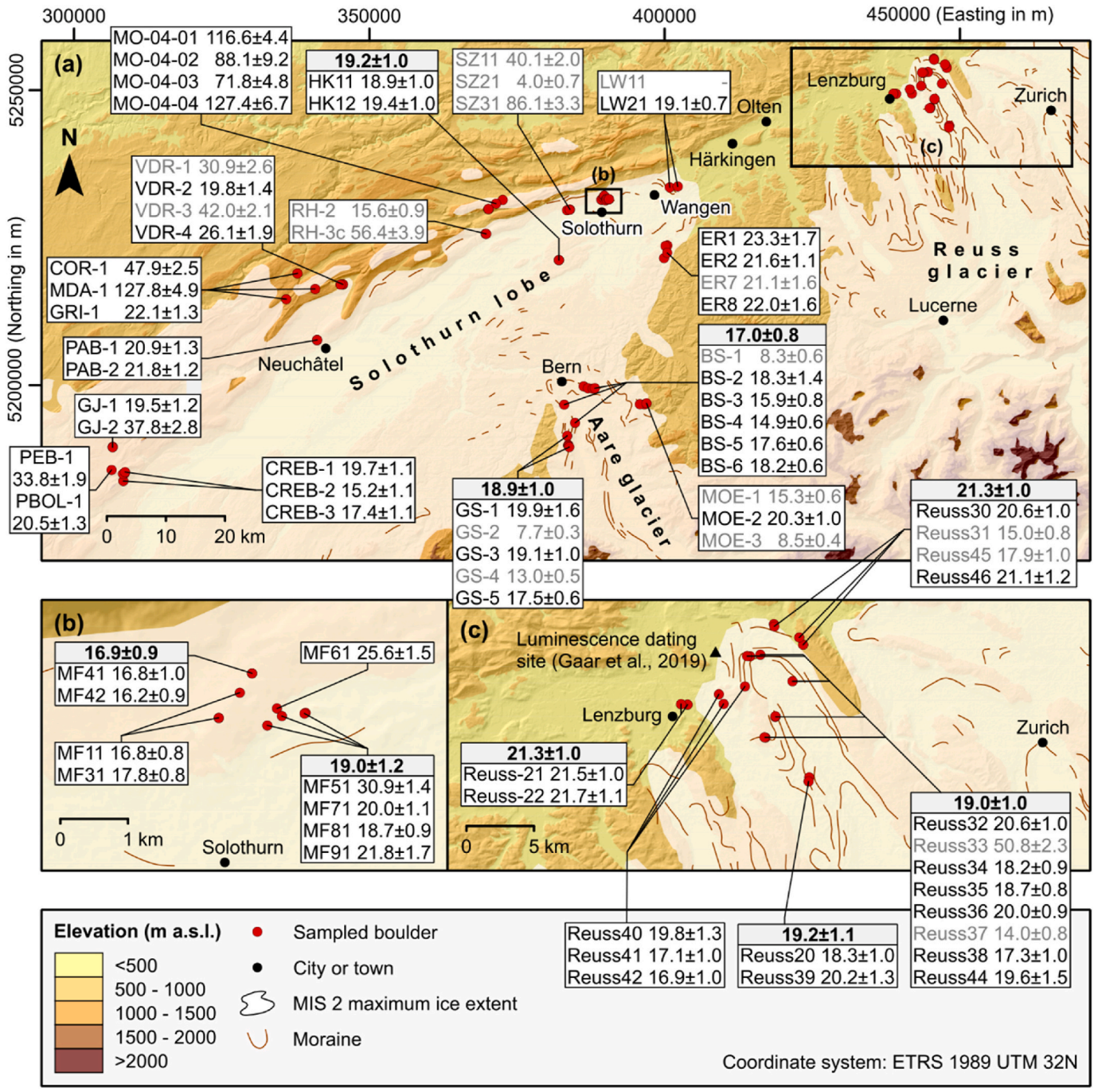

Fig. 5. Topographic map of the western part of the Swiss Plateau. For the MIS 2 maximum ice extent and moraines, see Ehlers et al. (2011), and Institut für Geologie, Universität Bern, Bundesamt für Wasser und Geologie (2005) respectively. For the data source of the elevation data in the background, see the caption of Fig. 1. Newly acquired and recalculated CRE ages of erratic boulders and associated external uncertainties are given in ka before 2010 CE and ka, respectively. Ages in grey were excluded in the original publications. For references to the original publications, see the main text.

et al., 2002) provide bracketing ages for the moraines of the Solothurn position. According to these ages, moraine formation occurred at the earliest at 20.2 ± 1.5 ka, but not later than 17.8—17.1 ka. The recalibrated basal age from Lake Neuchâtel reinforces the hypothesis that glacier recession from the Brästenberg position began no later than 20.2 ± 1.2 ka and not by 16.9 ± 0.9 ka at the latest. Given that Lake Neuchâtel is situated about 50 km south-west of the moraines at the Brästenberg position, it is unlikely that the region around Lake Neuchâtel was already ice free (no later than 17.8—17.1 ka) when the eastern branch of the Rhône glacier withdrew from these landforms.

5.3. *Comparison with existing chronologies from different parts of the Swiss Plateau*

We hereinafter compare the chronology of the last glaciation of the western Swiss Plateau with chronologies from Aare and the Reuss valleys. This comparison is based on newly acquired ages as well as recalculated ^{10}Be CRE ages for the Reuss and the Aare valleys (Table 3). Then, we compare the chronologies and propose possible stratigraphical correlations (Table 5).

According to optically stimulated and infrared-stimulated luminescence ages, glacio-fluvial and glacio-lacustrine sediments near the MIS 2

Table 4
Basal radiocarbon ages of lakes inside the MIS 2 maximum extent of the eastern lobe of the Rhône glacier. See Fig. 1 for the location of the lakes.

Lake	Basal ^{14}C age (a BP)	Basal age (cal. a BP)	Calibrated basal age (ka before 2010 CE)	Reference
Burgäschisee	15380 ± 70	18840–18330	18.9–18.4	Rey et al. (2017)
Moossee	15900 ± 130	19500–18910	19.6–19.0	Rey et al. (2020)
Lake Neuchâtel	14250 ± 95	17720–17060	17.8–17.1	Hadorn et al. (2002)

maximum position of the Reuss piedmont glacier (Fig. 5) were deposited at 25.1 ± 2.4 ka and 24.2 ± 2.2 ka, respectively (Gaar et al., 2019). Glacier retreat from the morphologically indistinct moraines at the maximum MIS 2 position of the Reuss glacier, the Untertannwald ice-marginal position, was underway by 21.3 ± 1.0 ka, as indicated by the mean age of the Reuss-21, Reuss-22, Reuss30, and Reuss46 boulders (recalculated from Reber et al., 2014; Kamleitner et al., 2023). Erratic boulders on the Wagenrain Molasse ridge inside the Untertannwald ice-marginal position stabilised no later than 19.8 ± 1.3 ka, as indicated by the CRE age of the Reuss40 boulder. The moraines at the Mellingen position formed during a subsequent period of ice-marginal stability or a glacier re-advance no later than 19.0 ± 1.0 ka (recalculated from Kamleitner et al., 2023). Subsequent glacier retreat was interrupted when the moraines at the Stetten ice-marginal position formed. According to CRE ages of the Reuss-20 and Reuss39 boulders, glacier recession from the moraines at this ice-marginal position began by 19.2 ± 1.1 ka at the latest (recalculated from Reber et al., 2014; Kamleitner et al., 2023). The moraines at the Bremgarten position (yet undated) further upstream crosscut moraines at the Stetten position, thus indicating a glacier re-advance. The Reuss glacier finally withdrew from the Swiss Plateau (Kamleitner et al., 2023).

The onset of the retreat of the Aare glacier from its MIS 2 maximum position remains largely unknown. The MOE-2 erratic boulder on Möschberg, a glacially formed Molasse ridge covered by glacial deposits, lies a few hundreds of meters inside the assumed MIS 2 maximum extent of the Aare glacier (Fig. 5; Bini et al., 2009) and yielded a (recalculated) CRE age of 20.3 ± 1.0 ka (Akçar et al., 2011). The retreat of the Aare glacier to the fringe of the Alps was interrupted by six major phases of ice-marginal stability. Commonly accepted ice-marginal positions of the Aare glacier are, from the oldest to the youngest, the Seftigschwand, Gurten/Gurtendörfli, Bern, Schlosshalde, Wittigkofen, and Muri positions (cf., Zienert, 1979; Gruner, 2001; Isler, 2005; Wüthrich et al., 2018). According to CRE ages of the GS-1, GS-3, and GS-5 erratic boulders, glacier retreat from the Gurten position was underway by 18.9 ± 1.0 ka at the latest (recalculated from Wüthrich et al., 2018). As emphasised by Wüthrich et al. (2018), the Aare and Rhône glaciers were still merged. A subsequent phase of ice-marginal stability or a glacial re-advance is documented by the morphologically distinct terminal moraines at the Bern position (cf., Nussbaum, 1921). During moraine formation, the Aare and Rhône glacier were already separated (Nussbaum, 1921; Krayss, 1989). Recalculated CRE ages from Wüthrich et al. (2018) indicate that glacier recession from the landforms began by 17.0 ± 0.8 ka at the latest.

Krayss (1989) already attempted to stratigraphically correlate ice-marginal positions of the eastern branch of the Rhône glacier with those of the Aare glacier. He mapped meltwater channels at the south-eastern margin of the eastern lobe of the Rhône glacier and in front of the Aare glacier. Krayss (1989) related these landforms based on their topographic position. During the formation of the moraines at the Gurten position, an ice-marginal channel apparently stretched from the area north-east of Bern (where the Aare glacier met the Rhône glacier) along the south-eastern margin of the eastern lobe of the Rhône glacier to Solothurn. The orientation of the ice-marginal channel would support the idea that the Solothurn and Gurten positions are of a similar age. During the formation of the moraines at the Bern position, ice-marginal channels apparently extended from the front of the Aare glacier in a north-westerly direction to the south-eastern margin of the Rhône glacier and continued in a north-easterly direction to a former lake (Krayss, 1989) that formed in the overdeepened Aare Valley upstream from Solothurn (Ledermann, 1991; Bläsi et al., 2015). It should be noted that, due to the lack of chronological data, the spatial relations proposed by Krayss (1989) should be considered with caution and that some of the channels might be polygenetic, i.e., subglacial channels may have evolved into ice-marginal channels. Once the moraines at the Solothurn position are dated, it will be possible to answer the question of whether these landforms and moraines at the Gurten or Bern position are of a similar age.

According to the presented CRE ages, the eastern branch of the Rhône glacier withdrew from the Brästenberg position no later than 20.2 ± 1.2 ka. We regard the CRE age of a boulder close to the MIS 2 maximum position of the Aare glacier (20.3 ± 1.0 ka) as an indication that the Aare Glacier had possibly not yet reached its MIS 2 maximum extent by 20.2 ± 1.2 ka at the latest. Time-transgressive MIS 2 maximum positions of the Aare and Rhône glaciers would not be surprising, since the accumulation area of the Rhône glacier was situated south of the main ice divide in the Alps, whereas the accumulation area of the Aare glacier was situated north of the main ice divide. As there is compelling evidence that humid air masses from the Mediterranean Sea mainly triggered the MIS 2 maximum glacier advance of several glaciers in the Alps (e.g., Florineth and Schlüchter, 2000; Kuhlemann et al., 2008; Luetscher et al., 2015; Monegato et al., 2017), it is plausible to assume

Table 5
Ice-marginal positions of the eastern lobe of the Rhône glacier (Bläsi et al., 2015), the Aare glacier (Gruner, 2001; Isler, 2005), and the Reuss glacier (Kamleitner et al., 2023), and minimum ages for ice recession from ice-marginal positions.

Rhône glacier			Aare glacier			Reuss glacier		
Ice-marginal position	Minimum age (ka)		Ice-marginal position	Minimum age (ka)		Ice-marginal position	Minimum age (ka)	
Langenthal	?		Bantiger *sensu* Gerber (1955)	?		Untertannwald	21.3 ± 1.0	[d]
Niederbipp	19.1 ± 0.7	[a]	Seftigschwand	?		Mellingen	19.0 ± 1.0	[d]
Hobiel	?		Gurten	18.9 ± 1.0	[c]	Stetten	19.2 ± 1.1	[d]
Brästenberg	20.2 ± 1.2	[a]	Bern	17.0 ± 0.8	[c]	Bremgarten	?	
Solothurn	20.2 ± 1.2 to 17.8—17.1	[a] [b]	Schlosshalde	?				
			Wittigkofen	?				
			Muri	?				

[a] This study.
[b] Recalibrated from Hadorn et al. (2002).
[c] Recalculated from Wüthrich et al. (2018).
[d] Recalculated from Reber et al. (2014) and Kamleitner et al. (2023).

that the Aare glacier reached its maximum when the polar front over the Atlantic Ocean shifted northwards and the Atlantic Ocean became the predominant moisture source for Central Europe. Since the minimum age of glacier recession from the MIS 2 maximum position of the Aare glacier (20.3 ± 1.0 ka) is currently only backed up by one CRE age, additional chronological data is urgently needed.

Due to their location in similar morphostratigraphic positions, the moraines at the Langenthal, Niederbipp, Brästenberg, and Solothurn positions might have formed at the same time as those at the Untertannwald, Mellingen, Stetten, and Bremgarten positions of the Reuss glacier, respectively (Fig. 6). According to recalculated and newly acquired CRE ages, it is possible that the eastern lobe of the Rhône glacier had already retreated to, at least, the moraines at the Brästenberg position when the Reuss glacier abandoned its MIS 2 maximum position (no later than 21.3 ± 1.0 ka). This possibility should be regarded as a working hypothesis for future studies. Determining the MIS 2 maximum position of the eastern branch of the Rhône glacier and obtaining a minimum age of the onset of glacier recession from this position will render possible testing this working hypothesis.

6. Conclusion

Beryllium-10 CRE dating allowed, for the first time, for directly dating the Niederbipp and Brästenberg positions of the eastern lobe of the Rhône glacier during the last deglaciation of the western part of the Swiss Plateau. The eastern branch of the Rhône glacier retreated by 19.1 ± 0.7 ka at the latest from the Niederbipp position. This piedmont lobe withdrew no later than 20.2 ± 1.2 ka, or alternatively, by 16.9 ± 0.9 ka at the latest from the moraines at the Brästenberg position. Erratic boulders at Martinsflue, outboard the Brästenberg position, gave ages conflicting with the stratigraphy. Due to scattering CRE ages of boulders on moraines at the Solothurn position, the timing of the onset of glacier retreat from this position could not be determined with CRE dating. However, the recalculated basal age of Lake Neuchâtel and the inferred minimum age of the Brästenberg position provide bracketing ages for the ice-marginal position. The eastern branch of the Rhône glacier abandoned the ice-marginal position at the earliest at 20.2 ± 1.2 ka, but not later than 17.8—17.1 ka.

Although this study provides valuable new insights into the chronology of the last deglaciation of the western Swiss Plateau, the deglaciation history is still far from being fully understood. Unrealistically old and incredibly young CRE ages lend credence to the idea that complex exposure histories of erratic boulders are prevalent in the study area. Carbon-14 CRE dating of the rock surfaces sampled for this study would be beneficial to complement this study and obtain valuable information on the deglaciation history of the western Swiss Plateau. Future research should also aim to determine the age of the Langenthal, Hobiel, and Solothurn positions of the eastern lobe of the Rhône glacier, as only the minimum ages of the Niederbipp and Brästenberg positions could be determined for this study. In addition, complementary data is needed to test the working hypothesis that glacier recession from the MIS 2 maximum positions of the Aare, Reuss and Rhône glaciers did not occur at the same time. Future research should aim to further constrain the MIS 2 maximum extent of the eastern branch of the Rhône glacier and the timing of the onset of glacier recession from the MIS 2 maximum position. As pointed out above, this could help to resolve the discrepancy between glacier extents predicted by glacier models and geomorphological/chronological evidence. As ^{10}Be CRE dating of erratic boulders on the Swiss Plateau has shown to be problematic due to a strong imprint of human activity, methods other than CRE dating for age

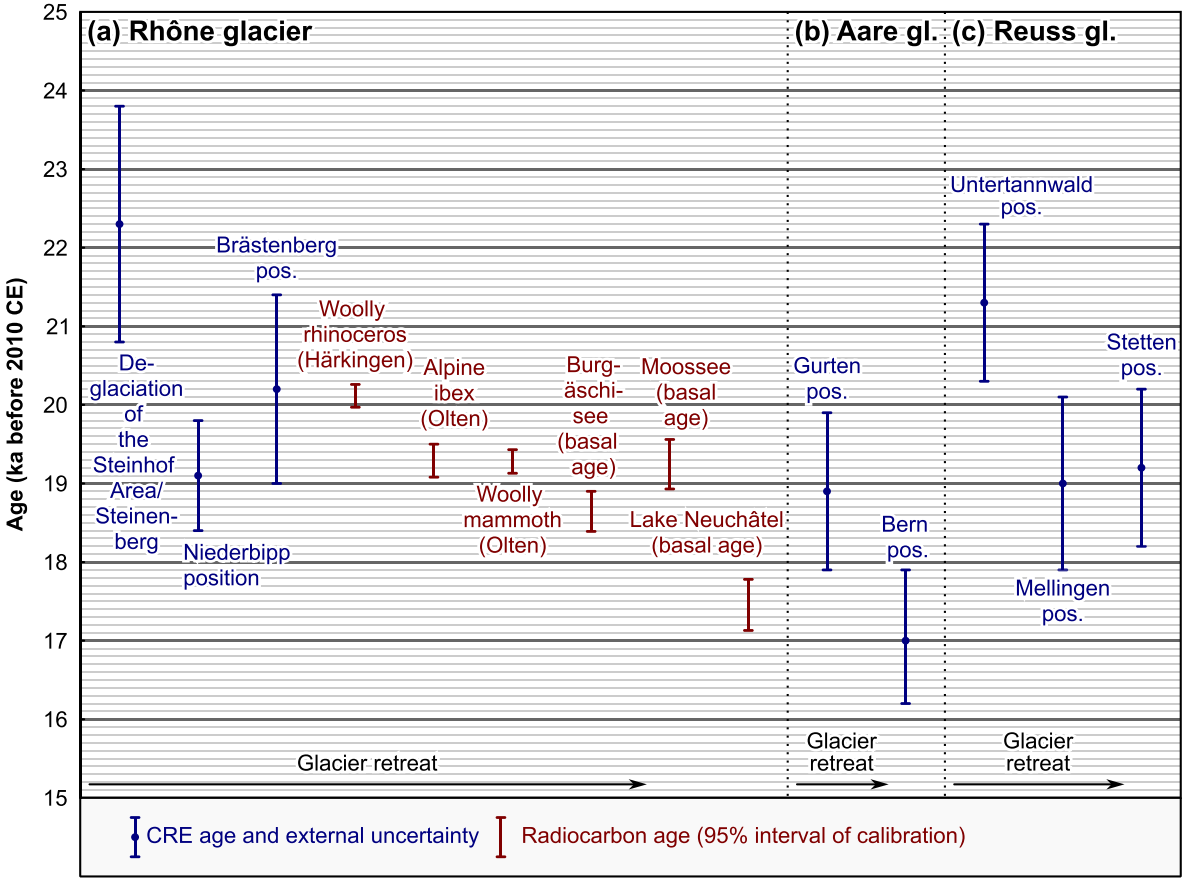

Fig. 6. Chronological data on the last deglaciation of the regions formerly covered by the Rhône, Aare, and Reuss glaciers. For the references, see the main text. Note that the magnitude of ice retreat is not shown in this figure, as the location of the MIS 2 maximum and Brästenberg positions of the Rhône glacier remains unknown.

determinations of glacial deposits and landforms, such as luminescence dating, should be applied in future studies.

Author contribution

RZ designed the study. The fieldwork was undertaken by RZ and CG. EGM, ARG, JS, and RZ conducted laboratory work under the guidance of SM. SM, AS, and GR led the AMS measurements at Helmholtz-Zentrum Dresden – Rossendorf. FMH, ARG, and EGM processed and analysed the data. FMH created the figures and drafted the manuscript with contributions from ARG. All authors contributed to the interpretation of the data and the final version of the manuscript.

Declaration of competing interest

The authors declare that they have no known competing financial interests or personal relationships that could have appeared to influence the work reported in this paper.

Data availability

All relevant data supporting the findings of this study are given in the supplement. All other data will be made available from the corresponding author upon request.

Acknowledgements

This research was financially supported by the Swiss National Science Foundation, Switzerland (SNSF; grant no.: PP00P2 150590). This work was undertaken while Felix Martin Hofmann was in receipt of a PhD studentship of *Studienstiftung des Deutschen Volkes*. The reviewers are thanked for their constructive comments which resulted in considerable improvements to the manuscript.

Appendix A. Supplementary data

Supplementary data to this article can be found online at https://doi.org/10.1016/j.qsa.2023.100124.

References

Akçar, N., Ivy-Ochs, S., Kubik, P.W., Schlüchter, C., 2011. Post-depositional impacts on 'Findlinge' (erratic boulders) and their implications for surface-exposure dating. Swiss J. Geosci. 104, 445–453. https://doi.org/10.1007/s00015-011-0088-7.

Akhmadaliev, S., Heller, R., Hanf, D., Rugel, G., Merchel, S., 2013. The new 6MV AMS-facility DREAMS at Dresden. Nucl. Instrum. Meth. B 294, 5–10. https://doi.org/10.1016/j.nimb.2012.01.053.

Antenen, M., Kellerhals, P., Tröhler, B., 2004. Blatt 1126 Büren a. A., mit Beiträgen von R. Schürch. - Geol. Atlas Schweiz 1:25 000, Karte 109. Bundesamt für Landestopografie swisstopo, Wabern.

Balco, G., 2016. ^{26}Al-^{10}Be exposure age/erosion rate calculators: table of Be and Al isotope ratio standardizations. http://hess.ess.washington.edu/math/docs/al_be_v22/AlBe_standardization_table.pdf. (Accessed 7 September 2022).

Balco, G., 2011. Contributions and unrealized potential contributions of cosmogenic-nuclide exposure dating to glacier chronology, 1990–2010. Quat. Sci. Rev. 30, 3–27. https://doi.org/10.1016/j.quascirev.2010.11.003.

Balco, G., Stone, J.O., Lifton, N.A., Dunai, T.J., 2008. A complete and easily accessible means of calculating surface exposure ages or erosion rates from ^{10}Be and ^{26}Al measurements. Quat. Geochronol. 3, 174–195. https://doi.org/10.1016/j.quageo.2007.12.001.

Bini, A., Buoncristiani, J.F., Couterrand, S., Ellwanger, D., Felber, M., Florineth, D., Graf, H.R., Keller, O., Kelly, M., Schlüchter, C., Schoeneich, P., 2009. Switzerland during the Last Glacial Maximum 1: 500,000. Federal Office of Topography swisstopo, Wabern.

Bläsi, H.-R., Gygi, R., Gnägi, C., Graf, H.R., Jordan, P., Laubscher, H.P., Ledermann, H., Herold, T., Schlanke, S., Burkhalter, R., Kälin, D., 2015. Blatt 1107 Balsthal. Geol. Atlas Schweiz 1, 25000. Erläut. 139, Wabern.

Boxleitner, M., Ivy-Ochs, S., Egli, M., Brandova, D., Christl, M., Maisch, M., 2019. Lateglacial and early Holocene glacier stages - new dating evidence from the Meiental in central Switzerland. Geomorphology 340, 15–31. https://doi.org/10.1016/j.geomorph.2019.04.004.

Braumann, S.M., Schaefer, J.M., Neuhuber, S.M., Reitner, J.M., Lüthgens, C., Fiebig, M., 2020. Holocene glacier change in the Silvretta Massif (Austrian Alps) constrained by a new ^{10}Be chronology, historical records and modern observations. Quat. Sci. Rev. 245, 106493 https://doi.org/10.1016/j.quascirev.2020.106493.

Bronk Ramsey, C., 2009. Bayesian analysis of radiocarbon dates. Radiocarbon 51, 337–360. https://doi.org/10.1017/S0033822200033865.

Charpentier, J. de, 1841. Essai sur les glaciers et sur le terrain erratique du bassin du Rhône. Ducloux, Lausanne.

Chmeleff, J., Blanckenburg, F. von, Kossrt, K., Jakob, D., 2010. Determination of the ^{10}Be half-life by multicollector ICP-MS and liquid scintillation counting. Nucl. Instrum. Meth. B 268, 192–199. https://doi.org/10.1016/j.nimb.2009.09.012.

Claude, A., Ivy-Ochs, S., Kober, F., Antognini, M., Salcher, B., Kubik, P.W., 2014. The Chironico landslide (Valle Leventina, southern Swiss Alps): age and evolution. Swiss J. Geosci. 107, 273–291. https://doi.org/10.1007/s00015-014-0170-z.

Cohen, K.M., Gibbard, P.L., 2019. Global chronostratigraphical correlation table for the last 2.7 million years, version 2019 QI-500. Quat. Int. 500, 20–31. https://doi.org/10.1016/j.quaint.2019.03.009.

Coutterand, S., Schoeneich, P., Nicoud, G., 2009. Le lobe glaciaire lyonnais au maximum würmien glacier du Rhône ou/et glaciers savoyards ? Collection EDYTEM. Cahiers de Géographie 8, 11–22. https://doi.org/10.3406/edyte.2009.1069.

Dürst Stucki, M., Schlunegger, F., 2013. Identification of erosional mechanisms during past glaciations based on a bedrock surface model of the central European Alps. Earth Planet Sci. Lett. 384, 57–70. https://doi.org/10.1016/j.epsl.2013.10.009.

Ehlers, J., Gibbard, P.L., Hughes, P.D. (Eds.), 2011. Quaternary Glaciations - Extent and Chronology: A Closer Look. Developments in Quaternary Sciences, vol. 15. Elsevier, Amsterdam, Oxford.

Florineth, D., Schlüchter, C., 2000. Alpine evidence for atmospheric circulation patterns in Europe during the last glacial maximum. Quat. Res. 54, 295–308. https://doi.org/10.1006/qres.2000.2169.

Gaar, D., Graf, H.R., Preusser, F., 2019. New chronological constraints on the timing of Late Pleistocene glacier advances in northern Switzerland. E&G Quaternary Sci. J. 68, 53–73. https://doi.org/10.5194/egqsj-68-53-2019.

Gegg, L., Preusser, F., 2023. Comparison of overdeepened structures in formerly glaciated areas of the northern Alpine foreland and northern central Europe. E&G Quaternary Sci. J. 72, 23–36. https://doi.org/10.5194/egqsj-72-23-2023.

Gerber, E., 1955. Ergebnisse glazialgeologischer Studien nordöstlich von Bern. Mitt. Naturforsc. Ges. Bern 12, 3–21. https://doi.org/10.5169/seals-319636.

Gerber, M.E., Wanner, J., 1984. Geologischer Atlas der Schweiz. Blatt 1128 Langenthal. Schweizerische Geologische Kommission, Bern.

Gnägi, C., Becker, D., Szidat, S., Geiger, P., Flückiger, P.F., 2023. Die eiszeitlichen Makroreste von Grosssäugern des Naturmuseums Olten – Gletschervorstösse des Rhonegletschers zwischen 50–20 ka und Rückschlüsse auf das Paläoklima. Mitteilungen/Naturforschende Gesellschaft des Kantons Solothurn 45, 117–142.

Gnägi, C., Flückiger, P.F., Szidat, S., Veit, H., 2021. Neue spätpleistozäne Säugerreste aus dem Raum Olten – Stiess der eiszeitliche Rhonegletscher um 44ka bis ins westliche Mittelland vor? Mitteilungen/Naturforschende Gesellschaft des Kantons Solothurn 44, 53–58.

Graf, A., Akçar, N., Ivy-Ochs, S., Strasky, S., Kubik, P.W., Christl, M., Burkhard, M., Wieler, R., Schlüchter, C., 2015. Multiple advances of alpine glaciers into the Jura mountains in the Northwestern Switzerland. Swiss J. Geosci. 108, 225–238. https://doi.org/10.1007/s00015-015-0195-y.

Gruner, U., 2001. Geologischer Atlas der Schweiz 1:25000, Blatt 1167 Worb: Erläuterungen (mit Beiträgen von R. Burkhalter), Bundesamt für Wasser und Geologie. Bern.

Hadorn, P., Thew, N., Russell Coope, G., Lemdahl, G., Hajdas, I., Bonani, G., 2002. A Late-Glacial and Early Holocene environment and climate history for the Neuchâtel region (CH). In: Équilibres et ruptures dans les ecosystemes depuis 20 000 ans en Europe de l'Ouest. Actes du colloque international de Besançon 18-22 septembre 2000, Besançon, pp. 75–90.

Haeberli, W., Schlüchter, C., 1987. Geological evidence to constrain modelling of the late Pleistocene Rhonegletscher (Switzerland). In: The Physical Basis of Ice Sheet Modelling (Proceedings of the Vancouver Symposium, August 1987), pp. 333–346. Vancouver.

Haeberli, W., 2005. Investigating glacier-permafrost relationships in high-mountain areas: historical background, selected examples and research needs. Geol. Soc., London, Special Publicat. 242, 29–37. https://doi.org/10.1144/GSL.SP.2005.242.01.03.

Hantke, R., 1977. Eiszeitliche Stände des Rhone-Gletschers im westlichen Schweizerischen Mittelland. Ber. Naturf. Ges. Freiburg i. Br. 67, 75–83.

Heiri, O., Koinig, K.A., Spötl, C., Barrett, S., Brauer, A., Drescher-Schneider, R., Gaar, D., Ivy-Ochs, S., Kerschner, H., Luetscher, M., Moran, A., Nicolussi, K., Preusser, F., Schmidt, R., Schoeneich, P., Schwörer, C., Sprafke, T., Terhorst, B., Tinner, W., 2014. Palaeoclimate records 60–8 ka in the Austrian and Swiss Alps and their forelands. Quat. Sci. Rev. 106, 186–205. https://doi.org/10.1016/j.quascirev.2014.05.021.

Hippe, K., 2017. Constraining processes of landscape change with combined in situ cosmogenic ^{14}C-^{10}Be analysis. Quat. Sci. Rev. 173, 1–19. https://doi.org/10.1016/j.quascirev.2017.07.020.

Hofmann, F.M., 2022. Technical note: Evaluating a geographical information system (GIS)-based approach for determining topographic shielding factors in cosmic-ray exposure dating. Geochronology 4, 691–712. https://doi.org/10.5194/gchron-4-691-2022.

Hofmann, F.M., Preusser, F., Schimmelpfennig, I., Léanni, L., ASTER Team, 2022. Late Pleistocene glaciation history of the southern Black Forest, Germany: ^{10}Be cosmic-ray exposure dating and equilibrium line altitude reconstructions in Sankt Wilhelmer Tal. J. Quat. Sci. 37, 688–706. https://doi.org/10.1002/jqs.3407.

Hofmann, F.M., Rauscher, F., McCreary, W., Bischoff, J.-P., Preusser, F., 2020. Revisiting Late Pleistocene glacier dynamics north-west of the Feldberg, southern Black forest,

Germany. E&G Quaternary Sci. J. 69, 61–87. https://doi.org/10.5194/egqsj-69-61-2020.
Hofmann, F.M., Alexanderson, H., Schoeneich, P., Mertes, J.R., Léanni, L., ASTER Team, 2019. Post-Last Glacial Maximum glacier fluctuations in the southern Écrins massif (westernmost Alps): insights from ^{10}Be cosmic ray exposure dating. Boreas 48, 1019–1041. https://doi.org/10.1111/bor.12405.
Hughes, P.D., Gibbard, P.L., 2015. A stratigraphical basis for the last glacial maximum (LGM). Quat. Int. 383, 174–185. https://doi.org/10.1016/j.quaint.2014.06.006.
Institut für Geologie, Universität Bern, Bundesamt für Wasser und Geologie, 2005. Geologische Karte der Schweiz 1:500 000. Bundesamt für Landestopografie swisstopo, Wabern.
Isler, A., 2005. Geologischer Atlas der Schweiz 1:25000, Blatt 1166 Bern: Erläuterungen, Bundesamt für Landestopografie. Bern.
Ivy-Ochs, S., 2015. Glacier variations in the European Alps at the end of the last glaciation. Cuadernos de Investigación Geográfica 41, 219–315. https://doi.org/10.18172/cig.2750.
Ivy-Ochs, S., 1996. The Dating of Rock Surfaces Using in Situ Produced ^{10}Be, ^{26}Al and ^{36}CI, with Examples from Antarctica and the Swiss Alps. Doctoral thesis, Swiss Federal Institute of Technology in Zurich, Zurich, p. 196.
Ivy-Ochs, S., Kober, F., 2008. Surface exposure dating with cosmogenic nuclides. E&G Quaternary Sci. J. 57, 179–209. https://doi.org/10.3285/eg.57.1-2.7.
Ivy-Ochs, S., Hippe, K., Schlüchter, C., 2021. The glacial landscape at Wangen an der Aare. In: Reynard, E. (Ed.), Landscapes and Landforms of Switzerland. Springer International Publishing, Cham, pp. 277–288. https://doi.org/10.1007/978-3-030-43203-4_19.
Ivy-Ochs, S., Kerschner, H., Reuther, A., Preusser, F., Heine, K., Maisch, M., Kubik, P.W., Schlüchter, C., 2008. Chronology of the last glacial cycle in the European Alps. J. Quat. Sci. 23, 559–573. https://doi.org/10.1002/jqs.1202.
Ivy-Ochs, S., Kerschner, H., Schlüchter, C., 2007. Cosmogenic nuclides and the dating of Lateglacial and Early Holocene glacier variations: the Alpine perspective. Quat. Int. 164–165, 53–63. https://doi.org/10.1016/j.quaint.2006.12.008.
Ivy-Ochs, S., Kerschner, H., Kubik, P.W., Schlüchter, C., 2006a. Glacier response in the European Alps to heinrich event 1 cooling: the Gschnitz stadial. J. Quat. Sci. 21, 115–130. https://doi.org/10.1002/jqs.955.
Ivy-Ochs, S., Kerschner, H., Reuther, A., Maisch, M., Sailer, R., Schaefer, J., Kubik, P.W., Synal, H.-A., Schlüchter, C., 2006b. The timing of glacier advances in the northern European Alps based on surface exposure dating with cosmogenic ^{10}Be, ^{26}Al, ^{36}Cl, and ^{21}Ne. In: Alonso-Zarza, A.M., Tanner, L.H. (Eds.), In Situ-Produced Cosmogenic Nuclides and Quantification of Geological Processes. Geological Society of America, Boulder. https://doi.org/10.1130/2006.2415(04).
Ivy-Ochs, S., Schäfer, J., Kubik, P.W., Synal, H.-A., Schlüchter, C., 2004. Timing of deglaciation on the northern Alpine foreland (Switzerland). Eclogae Geol. Helv. 97, 47–55. https://doi.org/10.1007/s00015-004-1110-0.
Jordi, H.A., Bitterli, T., Gerber, M.E., 2003. Blatt 1108 Murgenthal. - Geol. Atlas Schweiz 1:25 000, Karte 113. Bundesamt für Landestopografie swisstopo, Wabern.
Jouvet, G., Seguinot, J., Ivy-Ochs, S., Funk, M., 2017. Modelling the diversion of erratic boulders by the Valais Glacier during the last glacial maximum. J. Glaciol. 63, 487–498. https://doi.org/10.1017/jog.2017.7.
Kamleitner, S., Ivy-Ochs, S., Manatschal, L., Akçar, N., Christl, M., Vockenhuber, C., Hajdas, I., Synal, H.-A., 2023. Last Glacial Maximum glacier fluctuations on the northern Alpine foreland: geomorphological and chronological reconstructions from the Rhine and Reuss glacier systems. Geomorphology 423, 108548. https://doi.org/10.1016/j.geomorph.2022.108548.
Keller, O., Krayss, E., 2005. Der Rhein-Linth-Gletscher im letzten Hochglazial. 2. Teil: Datierung und Modelle der Rhein-Linth-Vergletscherung. Klima-Rekonstruktionen, Vierteljahrsschrift der Naturforschenden Gesellschaft in Zürich 150, 69–85.
Kelly, M.A., Buoncristiani, J.-F., Schlüchter, C., 2004. A reconstruction of the last glacial maximum (LGM) ice-surface geometry in the western Swiss Alps and contiguous Alpine regions in Italy and France. Eclogae Geol. Helv. 97, 57–75. https://doi.org/10.1007/s00015-004-1109-6.
Kohl, C., Nishiizumi, K., 1992. Chemical isolation of quartz for measurement of in-situ -produced cosmogenic nuclides. Geochem. Cosmochim. Acta 56, 3583–3587. https://doi.org/10.1016/0016-7037(92)90401-4.
Korschinek, G., Bergmaier, A., Faestermann, T., Gerstmann, U., Knie, K., Rugel, G., Wallner, A., Dillmann, I., Dollinger, G., Von Gostomski, C. L. von, 2010. A new value for the half-life of ^{10}Be by Heavy-Ion Elastic Recoil Detection and liquid scintillation counting. Nucl. Instrum. Meth. B 268, 187–191. https://doi.org/10.1016/j.nimb.2009.09.020.
Krayss, E., 1989. Modelle zu hochwürmzeitlichen Rückzugsphasen des Rhone-/Aaregletschers. Mitt. Naturforsc. Ges. Bern 46, 109–118. https://doi.org/10.5169/seals-318538.
Krüger, T., 2008. Die Entdeckung der Eiszeiten: Internationale Rezeption und Konsequenzen für das Verständnis der Klimageschichte, Wirtschafts-, Sozial- und Umweltgeschichte (WSU), vol. 1. Schwabe, Basel, p. 619.
Kuhlemann, J., Rohling, E.J., Krumrei, I., Kubik, P., Ivy-Ochs, S., Kucera, M., 2008. Regional synthesis of mediterranean atmospheric circulation during the last glacial maximum. Science 321, 1338–1340. https://doi.org/10.1126/science.1157638.
Lal, D., 1991. Cosmic ray labeling of erosion surfaces: in situ nuclide production rates and erosion models. Earth Planet Sci. Lett. 104, 424–439. https://doi.org/10.1016/0012-821X(91)90220-C.
Laubscher, H.P., Ledermann, H., Ford, J.R., Bläsi, H.-R., Gnägi, C., Kälin, D., 2014. Blatt 1107 Balsthal. Geol. Atlas Schweiz 1, 25000. Karte 139, Bundesamt für Landestopografie swisstopo, Wabern.
Le Roy, M., Deline, P., Carcaillet, J., Schimmelpfennig, I., Ermini, M., ASTER Team, 2017. ^{10}Be exposure dating of the timing of Neoglacial glacier advances in the Ecrins-Pelvoux massif, southern French Alps. Quat. Sci. Rev. 178, 118–138. https://doi.org/10.1016/j.quascirev.2017.10.010.
Ledermann, H., 1978. Geologischer Atlas der Schweiz. Blatt 1127 Solothurn. Erläuterungen, Bern.
Ledermann, H., 1977. Blatt 1127 Solothurn. - Geol. Atlas Schweiz 1: 25000. Schweizerische Geologische Kommission, Bern.
Ledermann, H., 1991. Über den „Solothurnersee. Mitteilungen/Naturforschende Gesellschaft des Kantons Solothurn 35, 213–231. https://doi.org/10.5169/seals-543384.
Li, Y., 2018. Determining topographic shielding from digital elevation models for cosmogenic nuclide analysis: a GIS model for discrete sample sites. J. Mt. Sci. 15, 939–947. https://doi.org/10.1007/s11629-018-4895-4.
Lisiecki, L.E., Raymo, M.E., 2005. A Pliocene-Pleistocene stack of 57 globally distributed benthic δ^{18}O records. Paleoceanography 20, PA1003. https://doi.org/10.1029/2004PA001071.
Luetscher, M., Boch, R., Sodemann, H., Spötl, C., Cheng, H., Edwards, R.L., Frisia, S., Hof, F., Müller, W., 2015. North atlantic storm track changes during the last glacial maximum recorded by alpine speleothems. Nat. Commun. 6, 6344. https://doi.org/10.1038/ncomms7344.
Mailänder, R., Veit, H., 2001. Periglacial cover-beds on the Swiss Plateau: indicators of soil, climate and landscape evolution during the Late Quaternary. Catena 45, 251–272. https://doi.org/10.1016/S0341-8162(01)00151-5.
Martin, L., Blard, P.-H., Balco, G., Lavé, J., Delunel, R., Lifton, N., Laurent, V., 2017. The CREp program and the ICE-D production rate calibration database: a fully parameterizable and updated online tool to compute cosmic-ray exposure ages. Quat. Geochronol. 38, 25–49. https://doi.org/10.1016/j.quageo.2016.11.006.
Maurer, E., 2005. "Im Interesse der Wissenschaft und zur Ehre des Landes" der Schutz der Findlinge im Kanton Bern. Mitt. Naturforsc. Ges. Bern 62, 135–159. https://doi.org/10.5169/seals-323882.
Merchel, S., Bremser, W., Bourlès, D.L., Czeslik, U., Erzinger, J., Kummer, N.-A., Leanni, L., Merkel, B., Recknagel, S., Schaefer, U., 2013. Accuracy of ^{9}Be-data and its influence on ^{10}Be cosmogenic nuclide data. J. Radioanal. Nucl. Chem. 298, 1871–1878. https://doi.org/10.1007/s10967-013-2746-x.
Millard, A.R., 2014. Conventions for reporting radiocarbon determinations. Radiocarbon 56, 555–559. https://doi.org/10.2458/56.17455.
Monegato, G., Scardia, G., Hajdas, I., Rizzini, F., Piccin, A., 2017. The Alpine LGM in the boreal ice-sheets game. Sci. Rep.-UK 7 (2078). https://doi.org/10.1038/s41598-017-02148-7.
Muscheler, R., Beer, J., Kubik, P.W., Synal, H.-A., 2005. Geomagnetic field intensity during the last 60,000 years based on ^{10}Be and ^{36}Cl from the Summit ice cores and ^{14}C. Quat. Sci. Rev. 24, 1849–1860. https://doi.org/10.1016/j.quascirev.2005.01.012.
NASA Jet Propulsion Laboratory, 2013. NASA Shuttle Radar Topography Mission Global 1 Arc Second. https://doi.org/10.5067/MEaSUREs/SRTM/SRTMGL1.003. (Accessed 31 May 2021).
Nishiizumi, K., Winterer, E.L., Kohl, C.P., Klein, J., Middleton, R., Lal, D., Arnold, J.R., 1989. Cosmic ray production rates of ^{10}Be and ^{26}Al in quartz from glacially polished rocks. J Geophys. Res.-Solid 94, 17907. https://doi.org/10.1029/JB094iB12p17907.
Nishiizumi, K., Imamura, M., Caffee, M.W., Southon, J.R., Finkel, R.C., McAninch, J., 2007. Absolute calibration of ^{10}Be AMS standards. Nucl. Instrum. Meth. B 258, 403–413. https://doi.org/10.1016/j.nimb.2007.01.297.
Nussbaum, F., 1921. Das Moränengebiet des diluvialen Aaregletschers zwischen Thun und Bern. Mitt. Naturforsc. Ges. Bern 42–84. https://doi.org/10.5169/seals-319288.
Nussbaum, F., 1951. Zur Kenntnis der Eiszeitbildungen der Umgebung von Solothurn. Mitt. Naturf. Ges. Solothurn 16, 1–44.
Ochs, M., Ivy-Ochs, S., 1997. The chemical behavior of Be, Al, Fe, Ca and Mg during AMS target preparation from terrestrial silicates modeled with chemical speciation calculations. Nucl. Instrum. Meth. B 123, 235–240. https://doi.org/10.1016/S0168-583X(96)00680-5.
Pfiffner, O.A., 2010. Geologie der Alpen, second ed., p. 360 Haupt, Bern, Stuttgart, Wien.
Pfirter, U., Antenen, M., Heckendorn, W., Burkhalter, R.M., Gürler, B., Krebs, D., 1996. Feuille 1106 Moutier. - Atlas Géol. Suisse 1:25 000, Carte 96. Bundesamt für Landestopografie swisstopo, Wabern.
Preusser, F., 1999. Lumineszenzdatierung fluviatiler Sedimente: Fallbeispiele aus der Schweiz und Norddeutschland. Kölner Forum für Geologie und Paläontologie 3, 62. Geologisches Institut der Universität Köln, Köln.
Preusser, F., Graf, H.R., Keller, O., Krayss, E., Schlüchter, C., 2011. Quaternary glaciation history of northern Switzerland. E&G Quaternary Sci. J. 60, 282–305. https://doi.org/10.3285/eg.60.2-3.06.
Preusser, F., Reitner, J.M., Schlüchter, C., 2010. Distribution, geometry, age and origin of overdeepened valleys and basins in the Alps and their foreland. Swiss J. Geosci. 103, 407–426. https://doi.org/10.1007/s00015-010-0044-y.
Preusser, F., Blei, A., Graf, H.R., Schlüchter, C., 2007. Luminescence dating of Würmian (Weichselian) proglacial sediments from Switzerland: methodological aspects and stratigraphical conclusions. Boreas 36, 130–142. https://doi.org/10.1111/j.1502-3885.2007.tb01187.x.
Reber, R., Akçar, N., Ivy-Ochs, S., Tikhomirov, D., Burkhalter, R., Zahno, C., Lüthold, A., Kubik, P.W., Vockenhuber, C., Schlüchter, C., 2014. Timing of retreat of the Reuss glacier (Switzerland) at the end of the last glacial maximum. Swiss J. Geoscci. 107, 293–307. https://doi.org/10.1007/s00015-014-0169-5.
Reimer, P.J., Austin, W.E.N., Bard, E., Bayliss, A., Blackwell, P.G., Bronk Ramsey, C., Butzin, M., Cheng, H., Edwards, R.L., Friedrich, M., Grootes, P.M., Guilderson, T.P., Hajdas, I., Heaton, T.J., Hogg, A.G., Hughen, K.A., Kromer, B., Manning, S.W., Muscheler, R., Palmer, J.G., Pearson, C., van der Plicht, J., Reimer, R.W., Richards, D.A., Scott, E.M., Southon, J.R., Turney, C.S.M., Wacker, L., Adolphi, F., Büntgen, U., Capano, M., Fahrni, S.M., Fogtmann-Schulz, A., Friedrich, R.,

Köhler, P., Kudsk, S., Miyake, F., Olsen, J., Reinig, F., Sakamoto, M., Sookdeo, A., Talamo, S., 2020. The IntCal20 Northern hemisphere radiocarbon age calibration Curve (0–55 cal kBP). Radiocarbon 62, 725–757. https://doi.org/10.1017/RDC.2020.41.

Rey, F., Gobet, E., Schwörer, C., Hafner, A., Szidat, S., Tinner, W., 2020. Climate impacts on vegetation and fire dynamics since the last deglaciation at Moossee (Switzerland). Clim. Past 16, 1347–1367. https://doi.org/10.5194/cp-16-1347-2020.

Rey, F., Gobet, E., van Leeuwen, J.F.N., Gilli, A., van Raden, U.J., Hafner, A., Wey, O., Rhiner, J., Schmocker, D., Zünd, J., Tinner, W., 2017. Vegetational and agricultural dynamics at Burgäschisee (Swiss Plateau) recorded for 18,700 years by multi-proxy evidence from partly varved sediments. Veg. Hist. Archaeobotany 26, 571–586. https://doi.org/10.1007/s00334-017-0635-x.

Rugel, G., Pavetich, S., Akhmadaliev, S., Enamorado Baez, S.M., Scharf, A., Ziegenrücker, R., Merchel, S., 2016. The first four years of the AMS-facility DREAMS: status and developments for more accurate radionuclide data. Nucl. Instrum. Meth. B 370, 94–100. https://doi.org/10.1016/j.nimb.2016.01.012.

Ruszkiczay-Rüdiger, Z., Kern, Z., Urdea, P., Madarász, B., Braucher, R., 2021. Limited glacial erosion during the last glaciation in mid-latitude cirques (Retezat Mts, Southern Carpathians, Romania). Geomorphology 384, 107719. https://doi.org/10.1016/j.geomorph.2021.107719.

Schwenk, M.A., Stutenbecker, L., Schläfli, P., Bandou, D., Schlunegger, F., 2022. Two glaciers and one sedimentary sink: the competing role of the Aare and the Valais glaciers in filling an overdeepened trough inferred from provenance analysis. E&G Quaternary Sci. J. 71, 163–190. https://doi.org/10.5194/egqsj-71-163-2022.

Seguinot, J., Ivy-Ochs, S., Jouvet, G., Huss, M., Funk, M., Preusser, F., 2018. Modelling last glacial cycle ice dynamics in the Alps. Cryosphere 12, 3265–3285. https://doi.org/10.5194/tc-12-3265-2018.

Stone, J.O., 2000. Air pressure and cosmogenic isotope production. J. Geophys. Res.-Solid 105, 23753–23759. https://doi.org/10.1029/2000JB900181.

Stroeven, A.P., Fabel, D., Hättestrand, C., Harbor, J., 2002. A relict landscape in the centre of Fennoscandian glaciation: cosmogenic radionuclide evidence of tors preserved through multiple glacial cycles. Geomorphology 44, 145–154. https://doi.org/10.1016/S0169-555X(01)00150-7.

Studer, B.: Beyträge zu einer Monographie der Molasse, Jenni, Bern, vol. 427 pp., 1825..

Uppala, S.M., Kållberg, P.W., Simmons, A.J., Andrae, U., Bechtold, V.D.C., Fiorino, M., Gibson, J.K., Haseler, J., Hernandez, A., Kelly, G.A., Li, X., Onogi, K., Saarinen, S., Sokka, N., Allan, R.P., Andersson, E., Arpe, K., Balmaseda, M.A., Beljaars, A.C.M., van Berg, L. de, Bidlot, J., Bormann, N., Caires, S., Chevallier, F., Dethof, A., Dragosavac, M., Fisher, M., Fuentes, M., Hagemann, S., Hólm, E., Hoskins, B.J., Isaksen, L., Janssen, P.A.E.M., Jenne, R., Mcnally, A.P., Mahfouf, J.-F., Morcrette, J.-J., Rayner, N.A., Saunders, R.W., Simon, P., Sterl, A., Trenberth, K.E., Untch, A., Vasiljevic, D., Viterbo, P., Woollen, J., 2005. The ERA-40 re-analysis. Q. J. R. Meteorol. Soc. 131, 2961–3012. https://doi.org/10.1256/qj.04.176.

Veit, H., Gnägi, C., 2014. Die Böden des Berner Mittellandes: Braunerden und Parabraunerden im Spiegel der eiszeitlichen Landschaftsentwicklung. In: Bäschlin, E., Mayer, H., Hasler, M. (Eds.), Bern: Stadt und Region: Die Entwicklung im Spiegel der Forschung, vols. 267–292. Geographische Gesellschaft Bern, Bern.

Wirsig, C., Zasadni, J., Christl, M., Akçar, N., Ivy-Ochs, S., 2016a. Dating the onset of LGM ice surface lowering in the High Alps. Quat. Sci. Rev. 143, 37–50. https://doi.org/10.1016/j.quascirev.2016.05.001.

Wirsig, C., Ivy-Ochs, S., Akçar, N., Lupker, M., Hippe, K., Wacker, L., Vockenhuber, C., Schlüchter, C., 2016b. Combined cosmogenic ^{10}Be, in situ ^{14}C and ^{36}Cl concentrations constrain Holocene history and erosion depth of Grueben glacier (CH). Swiss J. Geosci. 109, 379–388. https://doi.org/10.1007/s00015-016-0227-2.

Wüthrich, L., Morabito, E.G., Zech, J., Trauerstein, M., Veit, H., Gnägi, C., Merchel, S., Scharf, A., Rugel, G., Christl, M., Zech, R., 2018. ^{10}Be surface exposure dating of the last deglaciation in the Aare Valley, Switzerland. Swiss J. Geoscci. 111, 295–303. https://doi.org/10.1007/s00015-018-0298-3.

Wüthrich, L., Brändli, C., Braucher, R., Veit, H., Haghipour, N., Terrizzano, C., Christl, M., Gnägi, C., Zech, R., 2017. ^{10}Be depth profiles in glacial sediments on the Swiss Plateau: deposition age, denudation and (pseudo-) inheritance. E&G Quaternary Sci. J. 66, 57–68. https://doi.org/10.5194/egqsj-66-57-2017.

Zienert, A., 1979. Die Würmeisstände des Aaregletschers um Bern und Thun. In: Graul, H., Löscher, M. (Eds.), Sammlung Quartärgeomorphologischer Studien II. Geographisches Institut der Universität Heidelberg, Heidelberg, pp. 10–34.

Zimmermann, H.W., 1969. Zur Landschaftsgeschichte des Oberaargaus. Jahrbuch des Oberaargaus 12, 25–55.

Zimmermann, H.W., 1963. Die Eiszeit im westlichen zentralen Mittelland (Schweiz). Mitt. Naturf. Ges. Solothurn 21, 11–143. https://doi.org/10.5169/seals-543276.